Journal of Energy Storage 119 (2025) 116170

Contents lists available at ScienceDirect

Journal of Energy Storage

journal homepage: www.elsevier.com/locate/est

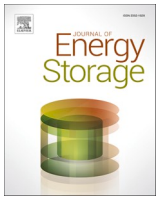

Research Papers

Hybrid energy storage power management system harnessing battery-supercapacitor synergy for grid-isolated DC microgrid

Jahidul Islam Shuvo [a], Md. Badoruzzaman [a], Shaikh Tawhidul Islam Anik [a], Shameem Ahmad [a], Tofael Ahmed [b], Mazaher Karimi [c,*]

[a] Department of Electrical and Electronic Engineering, American International University-Bangladesh, 1229 Dhaka, Bangladesh
[b] Department of Electrical and Electronic Engineering, Chittagong University of Engineering & Technology, Chattogram 4349, Bangladesh
[c] School of Technology and Innovations, University of Vaasa, FI-65200 Vaasa, Finland

ARTICLE INFO

Keywords:
Battery
Supercapacitor
Hybrid energy storage system
Dynamic energy management strategy
Electric vehicle
Stability
Microgrid

ABSTRACT

Energy storage systems (ESSs) are critical to the stability, reliability, and flexibility of microgrids (MGs). Dependence on a single ESS constrains operational longevity due to continuous cycling and difficulties in regulating swift load fluctuations. To address this, hybrid energy storage systems (HESSs) integrate various storage technologies, which are crucial for enhancing stability, efficiency, and operational performance of the system. Nonetheless, advanced power management strategies are essential for achieving optimal operation of HESSs due to their intricate characteristics. This study introduces a hybrid energy storage power management system (HESPMS) that integrates a HESS with an adaptive load management system designed for a grid-isolated solar-powered direct current (DC) MG. The adaptive load management component of the system actively equilibrates demand on the consumption side, efficiently controlling alternating current (AC) loads, such as residential loads, in addition to managing electric vehicle (EV) charging loads. The proposed HESPMS allows the SC to manage transients and the battery to supply continuous power, with one source compensating for the other when required, while adaptively aligning load demands with available solar and storage resources to enhance the performance and prolong the lifespan of HESS. Leveraging a fuzzy logic-based maximum power point tracking (MPPT) controller maximizes solar power conversion and generation efficiency. MATLAB/Simulink simulations validate the proposed system's robustness across multiple operational scenarios, demonstrating precise voltage regulation (±0.046), rapid settling time (20 ms), and peak overshoot of 2.53 %. These results underscore the system's resilience and ability to maintain stable operation under dynamic renewable energy conditions.

1. Introduction

The development of sustainable and resilient energy systems has enabled the integration via MGs to integrate renewable energy sources (RESs), such as solar and wind, into power grids. Implementing innovative solutions makes MGs an important component in regions with intermittent electricity supply. These systems effectively localize and reliably provide energy from renewable resources, create high-quality power supplies for communities, and increase resilience [1]. ESSs are key components of today's MGs that play an essential role in supplying reliable energy when outages occur and facilitate the smooth emergence of RESs [2]. ESSs attenuate the fluctuations and uncertainties associated with intermittent renewable generation, thereby stabilizing MGs and improving reliability as well as power quality while sustaining system performance [3]. This integration of ESSs brings economic benefits in terms of an improved energy balance and consumption during peak and off-peak hours, hence reducing operational costs by using advanced energy management algorithms that control energy distribution efficiently and support distributed generation sources [4]. ESSs enhance operational flexibility and resilience, thereby promoting sustainable MG performance across diverse environmental conditions and decreasing reliance on conventional energy sources [5].

ESSs are crucial for contemporary MGs; however, dependence on singular energy storage poses multiple challenges, such as elevated operational expenses, constrained lifespans, and complications in reconciling power density with energy capacity, thereby rendering MGs vulnerable to variations in load demand and renewable generation [6]. Batteries and SCs each possess inherent limitations, such as batteries

* Corresponding author at: School of Technology and Innovations, University of Vaasa, FI-65200 Vaasa, Finland.
E-mail address: mazaher.karimi@uwasa.fi (M. Karimi).

https://doi.org/10.1016/j.est.2025.116170
Received 1 December 2024; Received in revised form 22 February 2025; Accepted 9 March 2025
Available online 27 March 2025

delivering high energy density but exhibiting inadequate rate capability and diminished cycle stability during high-rate cycling, whereas SCs provide high power density and swift response but lack adequate energy capacity for prolonged supply [7]. These drawbacks subsequently result in operational losses, high maintenance needs, and a loss of reliability under diverse environmental conditions [8]. In addition, the above challenges are further exacerbated by the limited charging-discharging rates and rapid degradation because of their frequent usage [9]. Therefore, using these storage devices solely for both transient power demands and continuous energy requirements degrades the reliability and efficiency of the MGs [10]. HESSs combine different storage technologies to overcome the deficiencies of single-storage approaches, thus offering high power density and large energy capacity for high efficiency [11]. HESSs allow for swift responses to peak periods of demand, ensure a continuous supply of energy, and enhance the energy management, stability, and resilience of MGs with dynamic loads and varying renewable energy. Furthermore, it reduces operating costs and prolongs the lifespan of components by effectively reallocating loads between systems [12]. Nonetheless, HESS encounters considerable energy management challenges that arise from fluctuating supply and demand, which leads to instability, reduced durability of storage components, increased operational and control complexity, and issues in achieving optimal power control and reliable performance [13]. Another major concern for MGs is stability, as system oscillations, overshoots, and long settling times can disturb voltage, current, and power. Conventional controllers are commonly used owing to their straightforward design and ease of implementation. Nonetheless, they frequently fail to deliver consistent performance under dynamic and unpredictable conditions [14]. On the other hand, fuzzy-logic-based control systems ensure a high level of stability while being able to deal with the intrinsic uncertainty associated with renewable sources and variable loads [15]. Thus, the integration of advanced control algorithms is not only advantageous but also imperative, ensuring efficient power distribution, mitigating oscillations, decreasing stress on storage units, and markedly improving the overall system efficiency in DC MGs.

1.1. Existing works on hybrid energy storage systems

The literature review demonstrates recent developments and methodologies of hybrid energy storage power management in DC MG, highlighting their importance in improving the efficiency and dependability of the system. This study aims to identify the lapses and deficiencies of the current operational control schemes for power management in variable RESs and complex MG systems through a complete literature review.

S. Sinha and P. Bajpai (2020) developed an adaptive fuzzy logic controller (AFLC) for HESS in standalone DC MG to improve power-sharing by addressing inefficiencies in the conventional FLCs. The proposed AFLC faces challenges adapting rules quickly because of fast SoC changes thereby producing inefficient energy management and high discharge rates [16]. Prashant Singh and Jagdeep Singh Lather (2021) proposed a power management strategy (PMS) for a standalone DC MG with HESS to stabilize the DC-bus voltage and reduce stress on the battery. However, this PMS does not incorporate a real-time adaptive control mechanism to manage rapid load fluctuations, potentially affecting stability. Additionally, it exhibits limitations in precision regarding power-sharing between the battery and SC under varying loads. In addition, it does not comprehensively evaluate PMS performance in mixed-mode operations that necessitate coordinated management of the HESS [17].

Zineb Cabrane et al. (2021) proposed an energy management strategy for HESS, with a PI-based control strategy for DC bus voltage stabilization. Nevertheless, deficiencies persist in enhancing power-sharing, especially during peak demands, as evidenced by the slow battery reaction in simulation outcomes. The proposed control technique shows insufficient robustness in energy distribution between system components according to the power-sharing graphs obtained with various controller constants [18]. Arunkumar C.R. et al. (2022) proposed a voltage-based power distribution approach for a HESS in DC MG, incorporating a variable bandwidth low-pass filter (VBLPF) to enhance the SC utilization and extend battery lifespan. The proposed approach is deficient in a real-time adaptive control framework for rapid load fluctuations and offers a minimal assessment of its efficacy in stabilizing DC bus voltage amid varying SC charge levels. Moreover, there is no adequate HESS performance analysis in mixed-mode operations, considering the overlapped SC and battery contributions [19].

Ali Gaeed Seger Al-Salloomee et al. (2022) developed a standalone DC MG using a HESS with battery and SC to manage voltage transients under varying load and irradiance conditions. However, the study lacks comprehensive power-sharing optimization between the battery and SC, which may reduce operational efficiency. Additionally, this work also falls short in addressing the synchronization complexities inherent in dynamic load conditions, potentially leading to instability in real-time applications [20]. Remache, S et al. (2022) developed an optimal PMS for a DC MG with a HESS, where model predictive control (MPC) is used for power flow optimization and stability. A significant limitation is the employment of a constant 280 W load in simulations, which constrains the assessment of the HESS dynamic response capabilities, especially its capacity to manage rapid load variations [21].

Punna, S et al. (2022) developed a double-input bidirectional converter control strategy utilizing SC dynamics for stabilizing DC MG voltage during solar and load disturbances. The simulation models operate under restricted conditions regarding load and PV variations. The assessment of system resilience is limited because load failure conditions are excluded from analysis [22]. Furqan A. Abbas et al. (2022) devised an efficient energy management strategy (EMS) employing non-linear flatness control to regulate the DC bus voltage and improve power quality under fluctuating load conditions, thus optimizing MG performance. The proposed model EMS overlooks load failure scenarios, potentially resulting in system instability, voltage fluctuations, and considerable damage to the components [23].

Suchismita Patel et al. (2023) proposed a PMS developed to optimize the power distribution in HESS to address the demand-generation discrepancies, regulate DC bus voltage, and improve dynamic stability through a hybrid adaptive fuzzy PD-PI controller (HAFI FPD-PI). Nevertheless, the coordination between the HESS and RERs during simultaneous operation is insufficiently addressed, hence exposing a shortcoming in comprehensive power distribution management [24]. Shafiul Alam et al. (2023) have presented a small-signal modeling framework (SSMF) for synthesizing a fractional-order voltage compensation controller in a HESS for DC MG, where the control strategy has employed a modified particle swarm optimization (MPSO) technique with the objective of identifying optimum parameters for stable power sharing. Nonetheless, considerable synchronization complexity persists, affecting system performance. Moreover, although modification to droop controllers improves power-sharing efficiency, the accuracy of load distribution is still inadequate, indicating a need for additional advancements in control approaches to stabilize the bus voltage [25].

Hassan Abouobaida et al. (2023) proposed a hybrid energy management approach for a grid-isolated MG, which utilizes the fuzzy logic control (FLC) for MPPT and sliding mode control (SMC) to regulate power converters. This study is deficient in comprehensive evaluation under significant load fluctuations and renewable intermittency. It also depicts constrained power graph variations and limited load power scenarios while omitting the analysis of the HESS bidirectional operation, thereby reducing robustness [26]. S. Sruthi et al. (2024) proposed a hybrid energy management strategy integrating the mud ring algorithm (MRA) and FLC to enhance power sharing in DC MG for EV charging. However, the proposed control strategy does not have significant outcomes that demonstrate efficient energy management performance or load fluctuation, particularly for EV charging. Furthermore, it does not examine dynamic load conditions or the optimization of HESS [27].

1.2. Identified gaps in existing works

Table 1 summarizes the major energy management challenges in the existing control strategies for HESS in MG applications, which primarily focus on the optimization of power distribution, voltage stability, and dynamic load management. Some of the challenges are given below:

- Coordination challenges between HESS and RES disrupt seamless energy flow during simultaneous operations.
- Numerous investigations depend on limited simulations featuring constant loads and neglecting load failure condition analysis, which constrains understanding of system resilience.
- Inadequate energy distribution, elevated discharge rates, and delayed responses during peak times contribute to diminished performance.
- The absence of systematic assessments leaves the total system performance unquantified, whereas contributions to mixed-mode operation analyses remain substantially unexplored.
- Complex design of the controller and issues with synchronization prevent proper load balancing.
- The stability analysis of the controllers was not thoroughly conducted in most of the previous research works, leading to a lack of rigorous evaluation of the performance and reliability of the converters.

1.3. Contribution of the proposed work in overcoming existing limitations

These findings highlight the necessity to develop an innovative approach to improve the interaction between energy management and EV charging systems, thus increasing the stability, reliability, and efficiency of power sharing. The presented study comprehensively addresses these shortcomings by presenting an HESPMS that ensures a continuous power supply in grid-isolated DC MG via reliable and optimal energy allocation. The proposed fuzzy logic-based MPPT controller efficiently tackles the issues related to the utilization of PV and the stability of the DC link voltage which enhances the dynamic stability, voltage regulation, and its response to RES fluctuations than the conventional approaches. The proposed HESPMS optimizes energy allocation among the PV system, battery, SC, residential load, and EV charging load. Its effectiveness has been evaluated by efficient PV utilization, battery discharging, and SC discharging in order to maximize the performance of key MG components across multiple scenarios. This proposed HESPMS detects previously overlooked load variations and failure conditions, thereby enhancing system resilience and improving transient performance through system synchronization. This study uses Simulink within MATLAB to develop a complete simulation that evaluates system performance across various operational conditions. The findings indicate a significant enhancement in resilience and operational stability, especially for the management of fluctuating load demand in grid-isolated MG, with substantial implications for system robustness and dependability.

The primary objectives of this paper are outlined as follows:

- Developing a HESPMS aimed at optimizing power output and precisely regulating battery and SC charge-discharge cycles, ensuring reliable power continuity and enhanced system stability in a grid-isolated DC MG across variable operational scenarios.
- Implementing a fuzzy logic-based MPPT controller within the PV system to enhance real-time energy flow optimization in the HESPMS, effectively utilizing PV output and stabilizing DC link voltage amidst varying generation fluctuations.

Table 1
Literature review summary of control techniques and energy management approaches for HESS integrated grid-isolated DC MG:

Ref no.	Hybrid energy system control strategy	HESS combination	Controller stability analysis	THD analysis	Voltage regulation	Objectives	Limitations
[16]	AFLC	Battery + SC	–	–	> ± 5 %	Improve power sharing in HESS by addressing inefficiencies of conventional FLCs	1. Suboptimal energy allocation 2. High discharge rates
[17]	PMS with PI Controller	Battery + SC	✓	✓	> ± 5 %	Stabilizes DC bus voltage and reduces battery stress	1. No adaptive control for load shifts. 2. Lacks mixed-mode operation analysis
[18]	PI-Based Control Strategy	Battery + SC	–	–	<±10 %	Stabilizes DC bus voltage for HESS energy management	1. Slow battery response under peak loads. 2. Limits power-sharing effectiveness
[19]	Voltage-based powerdistribution with VBLPF	Battery + SC	✓	–	<±10 %	Enhances SC utilization, extends battery life	1. Lacks real-time adaptive control. 2. Minimal DC bus stabilization under SC charge variation
[20]	Voltage Transient Management	Battery + SC	–	–	–	Reduces DC voltage transients in MG under varying loads and irradiance	1. Lacks optimal power-sharing. 2. Synchronization challenge in dynamic loads
[21]	MPC-Based PMS	Battery + SC	–	–	> ± 5 %	Optimizes power flow and ensures stability for HESS	1. Constrained to a constant 280 W load. 2. Noisy DC bus voltage stability
[22]	Double-Input Bidirectional Converter	Battery + SC	✓	–	<±10 %	Stabilizes DC MG voltage by balancing power between battery and SC	1. Simulations limited to specific PV and load variations. 2. Excludes fault condition analysis
[23]	Flatness Non-linear Control Strategy	Battery +SC+ Fuel cell	–	–	> ± 5 %	Achieves high efficiency and stabilizes DC bus voltage	Inadequate stability of DC bus voltage
[24]	HAFI FPD-PI Controller	Battery + SC	✓	–	> ± 5 %	Enhances DC bus stability and battery lifespan	Complex design with tuning challenges
[25]	Fractional-Order Voltage Compensation with MPSO	Battery + SC	–	–	> ± 5 %	Optimizes power sharing and stabilizes DC bus voltage	1. Exhibits a sluggish response in stabilizing DC Bus voltage. 2. Insufficient load distribution accuracy
[26]	Fuzzy Logic with MPPT with SMC	Battery + SC	–	✓	> ± 5 %	Effective energy allocation and transient load management	1. Restricted load power scenarios. 2. Omitted bidirectional operation analysis of HESS
[27]	MRA with FLC	Battery + EV	–	–	–	Optimizes power sharing in DC MG for EV charging	1. No considerations regarding the SoC limit of the ESS. 2. Neglects EV charging performance

- Establishing a synergistic integration of the HESS with an adaptive load management strategy to enhance the efficiency and resilience of the proposed grid-isolated DC MG system, ensuring robust performance under real-time fluctuations compared to traditional systems.
- Validating the proposed HESPMS through four key operational scenarios—surplus energy with HESS charging, power shortfall with battery discharge, power shortfall with SC discharge, and power shortfall leading to load shedding—to assess its effectiveness in utilization and resilience.
- Conducting stability analysis of the controllers in the proposed system, such as the battery, SC, single-phase DC-AC inverter, and HESPMS controller, is essential to ensure system reliability and validate performance under diverse conditions. This evaluation aims to confirm the robustness of the presented controllers.

This paper is structured as follows: Section 2 outlines the modeling and control strategy of the proposed grid-isolated MG system. Section 3 demonstrates the stability analysis of the proposed system's controllers. Section 4 explains the operational modes and configuration of the grid-isolated DC MG, along with flowcharts as well as an analysis of the energy management strategy algorithm. Section 5 presents the simulation results of four different scenarios carried out in MATLAB/Simulink. Section 6 provides a comparative analysis. Lastly, Section 7 concludes the paper.

2. Modeling and control strategy of the proposed grid-isolated MG system

2.1. PV modeling

A PV system consists of a PV array modeled using the single-diode equivalent circuit of a PV cell. The output current of the PV cell is calculated by [28]:

$$I_{cell} = I_L - I_d\left(exp\left(\frac{V_{cell} + I_{cell}R_S}{aV_T}\right) - 1\right) - \frac{V_{cell} + R_S I_{cell}}{R_P} \tag{1}$$

$$I_d = I_{d.ref} - \left(\frac{T_{ref}}{T}\right)^3 \times exp\left(\frac{qE_{gap}}{ak}\left(\frac{1}{T_{ref}} - \frac{1}{T}\right)\right) \tag{2}$$

$$I_L = \frac{G}{G_a}\left(I_{L.ref} + V_{cell}\Delta T\right) \tag{3}$$

Here, Eq. (1) relates the output current I_{cell} to the light-generated current I_L, diode current I_d, and losses due to series resistance R_S and shunt resistance R_P. Eq. (2) defines I_d using the reference current $I_{d.ref}$, bandgap energy E_{gap}, thermal voltage V_t, electron charge q, Boltzmann constant k, and temperatures T and T_{ref}. Eq. (3) expresses I_L in terms of solar irradiance G, reference radiance G_a, reference light-generated current $I_{L.ref}$, temperature variation ΔT, and short-circuit voltage V_{cell}.

2.2. Battery modeling

To address the challenge of intermittent renewable energy, batteries are being explored as an effective energy storage solution. Fig. 1 illustrates the electrical equivalent circuit of the battery, along with its fundamental equations [29]:

$$V_{Bat} = V_o - k\frac{Q}{Q - it} + Aexp(-Bit) \tag{4}$$

$$V_{Bat} = V + R_{Bat}I_{Bat} \tag{5}$$

The state of charge (SoC) of the battery [29]:

$$SoC_{Bat} = SOC_{Bat} - \int_0^{-t} \eta i dt \tag{6}$$

In Eq. (4), V_{Bat} is the battery terminal voltage, V_o is the initial voltage, k is the polarization constant, Q is the capacity, i is the current, t is the discharge time, A is the exponential zone amplitude, and B is the inverse of the exponential zone time constant. Eq. (5) calculates the total output voltage V_{Bat} as the sum of V_{Bat} from Eq. (4), internal resistance R_{Bat}, and battery current I_{Bat}. Lastly, in Eq. (6) SoC_{Bat} is the SoC of the battery, η is the efficiency, i is the battery current, and the integral is a function for accumulated discharge over time.

2.3. SC modeling

Fig. 2 demonstrates the electrical equivalent circuit of an SC, elucidating its voltage responsiveness and energy storage characteristics via a controlled voltage source model [30].

$$V_T = \frac{N_s Q_T d}{N_p N_e \mathcal{E}\mathcal{E}_0 A_i} + \frac{2N_e N_s RT}{F} sin^{-1}\left(\frac{Q_T}{N_p N_e^2 A_i \sqrt{8RTe\mathcal{E}\mathcal{E}_0 c}}\right) \tag{7}$$

$$E_{SC,max} = \frac{1}{2}C_{sc}V_{SC,max}^2 \tag{8}$$

$$C_{sc}\frac{dV_{SC}}{dt} = -I_{SC} \tag{9}$$

In Eq. (7), V_T is the SC terminal voltage, N_s is the number of series units, Q_T is the total charge, N_p is the number of parallel units, $\mathcal{E}_0$ is the permittivity of free space, A_i is the electrode area, d is the electrode distance, N_e is the electron count, R is the gas constant, T is the temperature, F is Faraday's constant, and $\mathcal{E}$ is the electrolyte permittivity. In Eq. (8), $E_{SC,max}$ is the maximum energy stored in the SC, C_{sc} is the SC capacitance, and $V_{sc,max}$ is the maximum voltage. Eq. (9) defines $\frac{dV_{SC}}{dt}$ as the rate of voltage changes over time, and I_{SC} as the current through the SC.

2.4. Residential load modeling

Fig. 3 illustrates a circuit diagram of a residential load with an LC filter linked to a DC-AC inverter output, facilitating a smooth sinusoidal voltage at the load by eliminating switching ripples. Below are the equations for the inductor current, capacitor voltage, and load voltage behavior [31]:

$$L\frac{di_L(t)}{dt} = V_{inverter}(t) - V_c(t) \tag{10}$$

$$C\frac{dV_c(t)}{dt} = i_L(t) - i_{Load}(t) \tag{11}$$

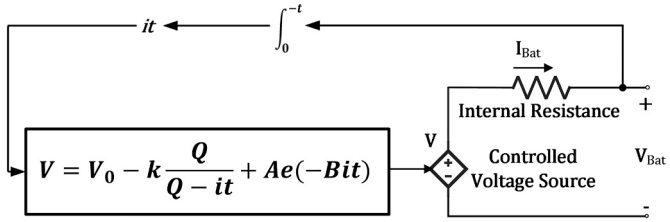

Fig. 1. The electrical equivalent circuit of battery [29].

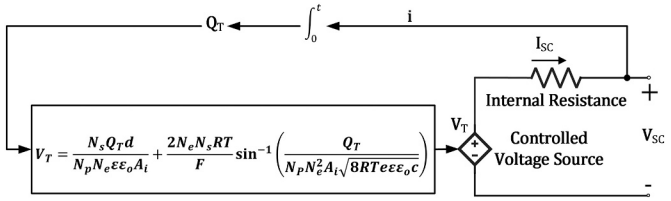

Fig. 2. The electrical equivalent circuit of SC [30].

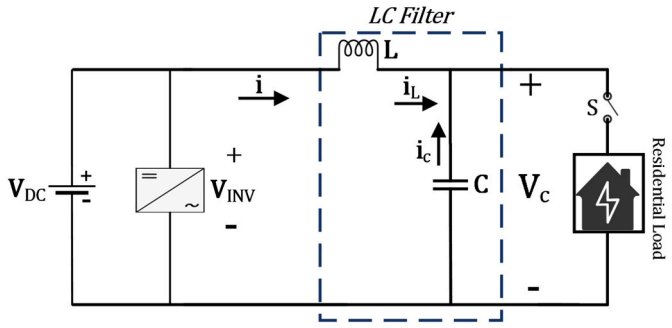

Fig. 3. The circuit diagram of residential load.

Power Balance at the Load:

$$P_{Load}(t) = V_c(t) \times i_{Load}(t) = \frac{V_c^2(t)}{R_{Load}} \tag{12}$$

Here, Eqs. (10) and (11) represent the inductor current and capacitor voltage, respectively. L is inductance, C is capacitance, $i_L(t)$ and $V_{inverter}(t)$ is inductor current and voltage, i_{Load} is current through the load, R_{Load} is the load resistance, $V_c(t)$ is the voltage across the load.

2.5. EV charger load modeling and control strategy

Fig. 4 illustrates the circuitry and control mechanism of a unidirectional DC-DC boost converter utilized in an EV charger. This method regulates the current from a DC bus to the EV charger by adjusting the duty cycle with pulse width modulation. The following are the equations of the system's behavior [32]:

$$L\frac{di_L(t)}{dt} = V_{DC} \times d(t) - V_{EV} \tag{13}$$

$$C\frac{dV_{EV}(t)}{dt} = i_L(t) - i_{EV}(t) \tag{14}$$

Eq. (13) represents the inductor current dynamics, and Eq. (14) capacitor voltage dynamics. Here, L is inductance, C is capacitance, $di_L(t)$ is the inductor current, V_{DC} is DC bus voltage, V_{EV} is output EV voltage, i_{EV} is EV charging current, $d(t)$ duty cycle from PWM. Here, K_p and K_i are proportional and integral gains.

Error Signal for power balance:

$$e_p = P_{Gen} - P_{Residentialload} - P_{EVload} \tag{15}$$

PI Controller output:

$$d(t) = K_p(i_{ref} - i_{EV}) + K_i \int (i_{ref} - i_{EV})dt \tag{16}$$

2.6. Single-phase inverter modeling and control strategy

Fig. 5 shows a single-phase full-bridge inverter converting DC to AC for the AC load using four switches ($S_1 - S_4$) in an H-bridge configuration. The general equations of a full bridge inverter are given below [33]:

$$V_{out}(t) = \frac{V_{DC}}{2}(m_a \times sin(\omega t)) \tag{17}$$

$$V_{out} = V_{DC} \times (S_1S_4 - S_2S_3) \tag{18}$$

In Eq. (17), V_{out} is the output voltage of the inverter, V_{DC} is the DC bus voltage, m_a is the modulation index, and ω is the angular frequency of the output AC signal. Eq. (18) describes the output voltage based on the switch states, where S_1, S_4, S_2, S_3 are the binary states (0 or 1) of the switches.

2.7. Proposed MPPT adaptive fuzzy logic integrated controller

Fig. 6 illustrates the block diagram of the MPPT system implementing an FLC. The controller uses the inputs ΔP_{PV} and ΔV_{PV} that are scaled by factors of α_1 and α_2 respectively. The controller generates an appropriate reference voltage $(V_{PV,ref})$ to the interfacing converter. These inputs are then processed by the FLC, comprising, in general, three major stages: fuzzification, which converts crisp inputs into fuzzy values; the fuzzy inference engine, which applies membership functions and rules; and defuzzification, which converts fuzzy outputs back to crisp values. The output $D[\alpha]$ ultimately regulates the duty cycle of the power converter for optimal performance under different situations.

The FLC rule Table 2 specifies control actions based on two inputs: the error e(t) and its variation d(t), with entries representing control outputs: EL (Extremely Low), ES (Extra Small), ZO (Zero), OS (Overshoot), and OL (Over Limit). This table serves as the basis for the fuzzy controller to facilitate the use of fine-tuning that is aimed at enhancing the performance of the system.

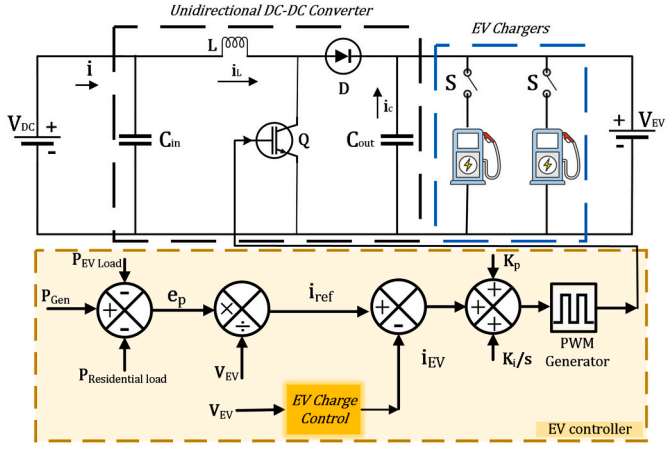

Fig. 4. Modeling and control of unidirectional DC-DC converter for EV charging [32].

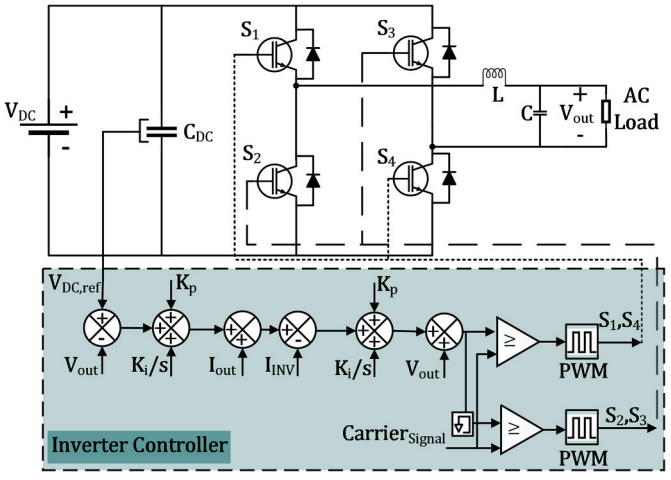

Fig. 5. Modeling and control of single-phase full bridge inverter.

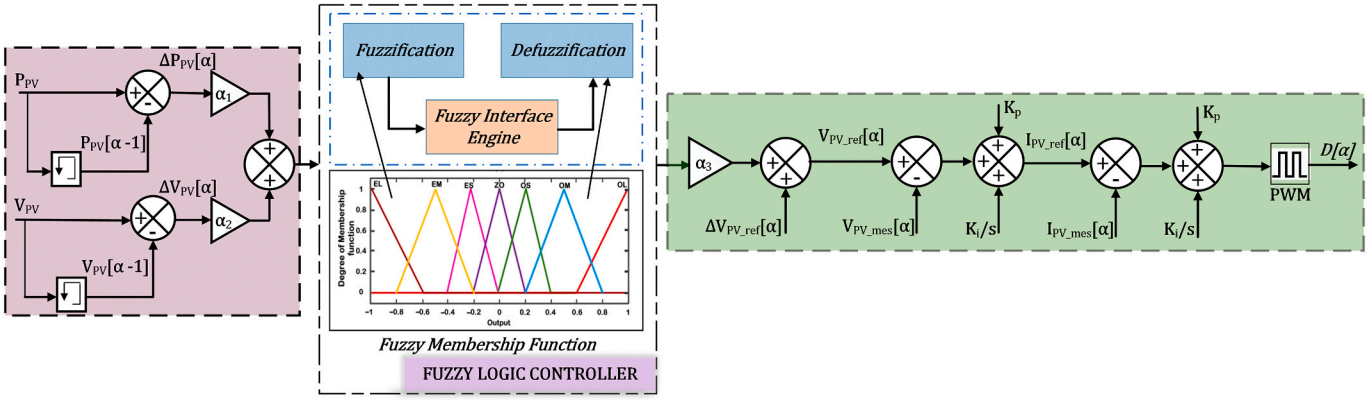

Fig. 6. Block diagram of MPPT-based FLC with membership function.

Table 2
FLC rule table.

e(t)	d(t)				
	EL	ES	ZO	OS	OL
EL	EL	EL	ES	ZO	OS
ES	EL	ES	ES	ZO	OL
ZO	ES	ES	ZO	OS	OL
OS	ZO	ZO	OS	OL	OL
OL	OS	OS	OL	OL	OL

2.8. Modeling of proposed HESPMS controller

The HESPMS controller demonstrated in Fig. 7 utilizes a fuzzy logic-based MPPT to optimize PV power extraction through analysis of power change rate (dP_{pv}/dt) and voltage change rate (dV_{pv}/dt). The power-sharing control structure depends on a hierarchical system that uses PI controllers with low-pass filters to regulate power distribution between PV, battery, and SC units. The battery and SC current controllers use limiting functions with SoC limits to maintain charging/discharging operations. The proposed HESPMS uses feedback loops to adjust reference currents (I_{ref}) which results in optimal power distribution. The bidirectional converters operate with PWM signals to ensure smooth power transfer and optimize system performance along with stability.

3. Stability analysis of the proposed system's controllers

This section provides a detailed stability analysis of the battery and SC controllers with a buck-boost configuration along with the single-phase inverter controller, to confirm the dynamic stability of the proposed system. Also, the stability of the proposed HESPMS controller is assessed through Bode plots, with its step response highlighting its superior performance compared to existing approaches. Such assessments further strengthen the effectiveness of the proposed control strategy in preserving system stability while maximizing system overall performance. The small-signal transfer functions governing the buck-boost operation of the battery and SC controllers are [34]:

$$G_{id}^{Boost}(s) = \frac{2V_{dc}}{RD_1}\left(\frac{1+sRC}{1+s\frac{L}{RD_1^2}+s^2LCD_1^2}\right) \tag{19}$$

$$G_{id}^{Buck}(s) = \frac{V_{ESS}}{RD_2}\left(\frac{1+sRC}{1+s\frac{L}{R}+s^2LC}\right) \tag{20}$$

For the single-phase inverter controller, the dynamics are [34]:

$$G_{vi}(s) = -\frac{V_{inverter}}{2C_{dc}V_{dc}s} \tag{21}$$

Table 3 shows the transfer functions derived by applying Eqs. (19)–(21) to the proposed battery converter and, SC converter and single-

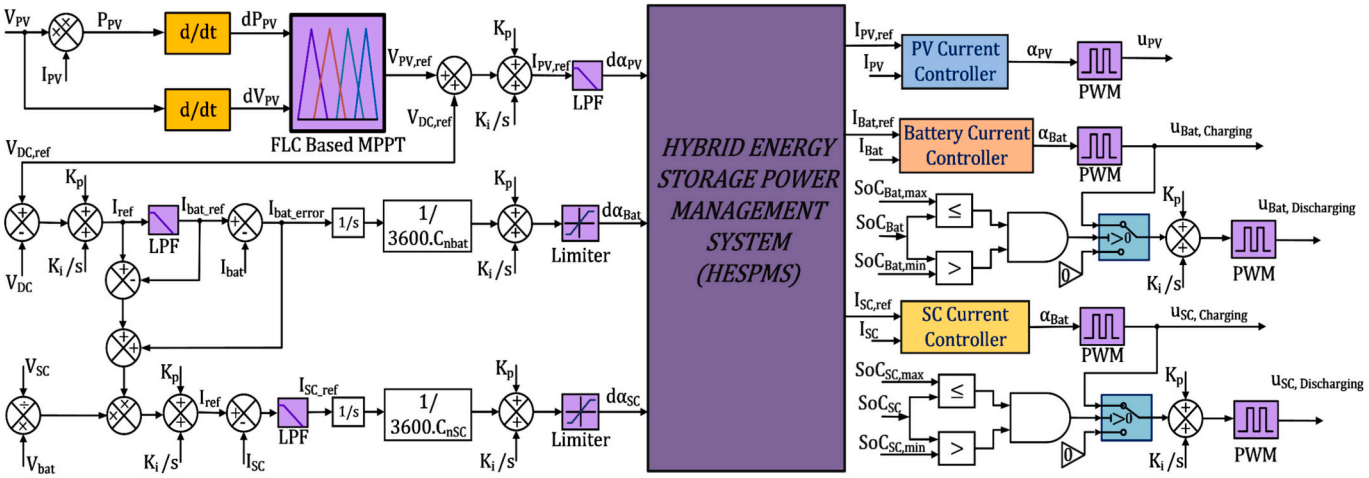

Fig. 7. Hybrid energy storage power management system (HESPMS) controller.

Table 3
Transfer functions of the proposed system controllers.

Components	Boost mode	Buck mode
Battery converter	$G_{bat}^{Boost}(s) = \frac{23(s+2.9\times10^5)}{0.0001917s^2+27.78s+30}$	$G_{bat}^{Buck}(s) = \frac{1.38s+200000}{2.76\times10^{-6}s^2+0.4s+50}$
SC converter	$G_{SC}^{Boost}(s) = \frac{23(s+2.9\times10^5)}{0.0001917s^2+27.78s+30}$	$G_{SC}^{Buck}(s) = \frac{2.53477s+369230.77}{2.76\times10^{-6}s^2+0.4s+40}$
DC-AC Inverter	$G_{INV}(s) = -\frac{694.44}{s}$	

phase DC-AC inverter controller. The transfer functions analyze the dynamic characteristics of each component, which helps understand stability and performance behavior.

3.1. Hybrid energy storage system stability analysis

The battery controller operates in Boost mode (a) and Buck mode (b) through comparison of $V_{Bat,ref}$ to V_{DC} to regulate output voltage shown in Fig. 8. PI controller G_{PI}^{Bat} handles the error signal to modify the battery current i_{Bat} while the battery converter dynamics are controlled by transfer functions $G_{Bat}^{Boost}(s)$ and $G_{Bat}^{Buck}(s)$ to maintain stable voltage regulation with proportional and integral gains K_p^{Bat} and K_i^{Bat}.

The Bode diagrams in Fig. 9 show the battery controller's performance in both Boost mode (a) and Buck mode (b). The compensated system in Boost mode provides better stability through higher gain while simultaneously reducing phase lag. The controller in Buck mode delivers enhanced phase margin together with smoother phase response and increased frequency stability across the range which surpasses the uncompensated system in both modes of operation.

The SC controller operates in Boost mode (a) and Buck mode (b) through a comparison of $V_{SC,ref}$ to V_{DC} to regulate output voltage as shown in Fig. 10. PI controller G_{PI}^{SC} handles the error signal to modify the

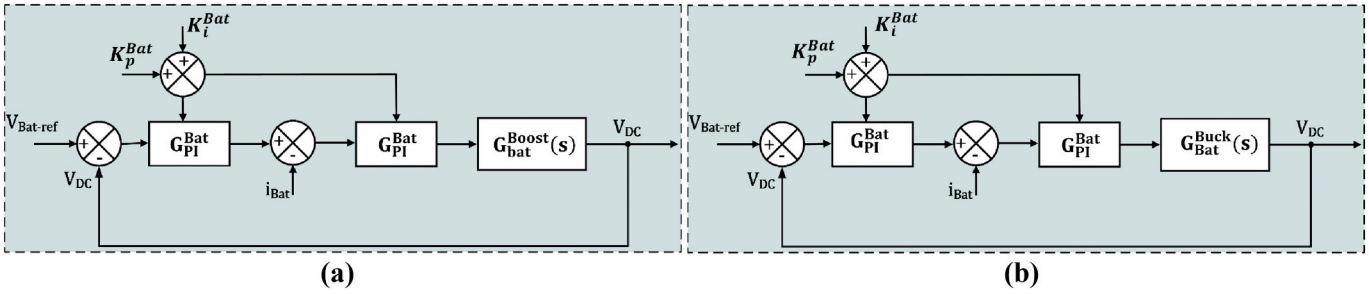

Fig. 8. Block diagram of closed loop battery controller (a) Boost mode (b) Buck mode.

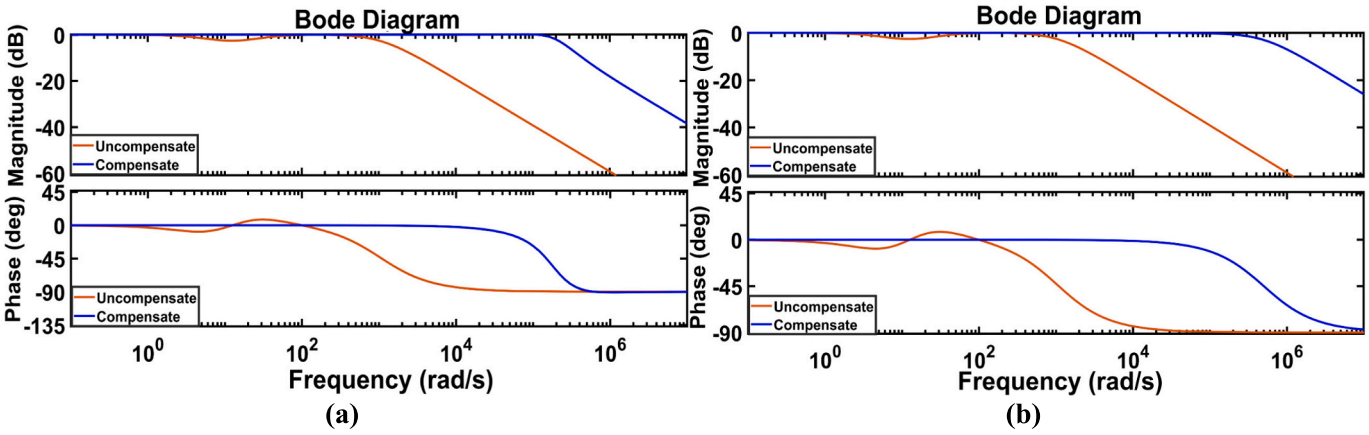

Fig. 9. Bode diagram of the battery controller (a) Boost mode (b) Buck Mode.

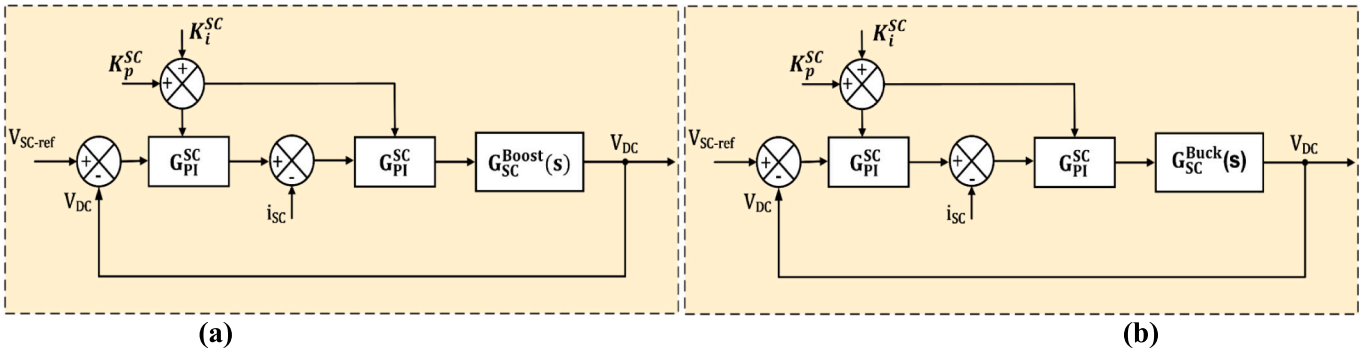

Fig. 10. Block diagram of closed loop SC controller (a) Boost mode (b) Buck mode.

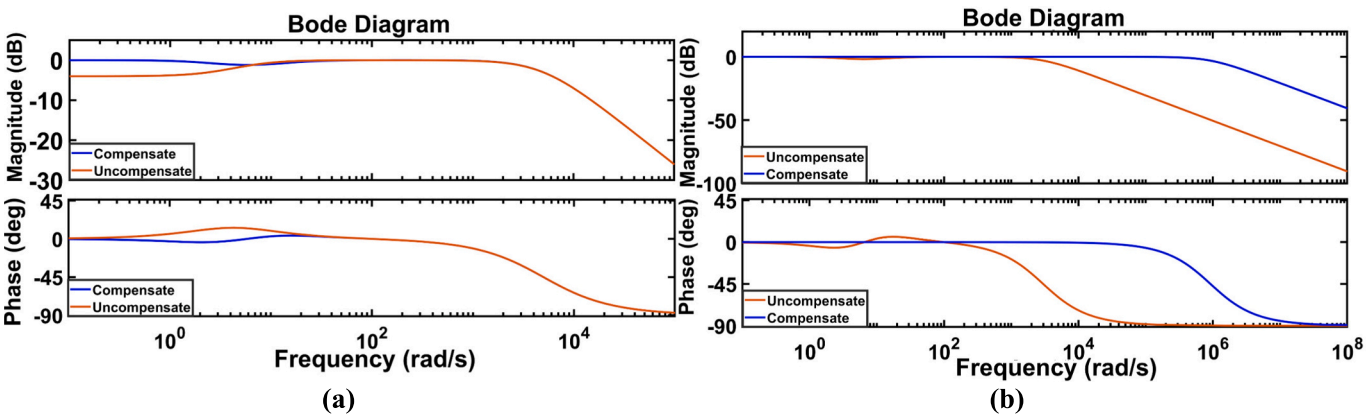

Fig. 11. Bode diagram of the SC controller (a) Boost mode (b) Buck Mode.

SC current i_{SC} while the SC converter dynamics are controlled by transfer functions $G_{SC}^{Boost}(s)$ and $G_{SC}^{Buck}(s)$ to maintain stable voltage regulation with proportional and integral gains K_p^{SC} and K_i^{SC}.

The Bode diagrams in Fig. 11 show the SC controller's performance in Boost mode (a) and Buck mode (b). In both modes, the compensated system offers higher stability, with better gain and phase margin compared to the uncompensated system. The compensated system also reduces phase lag at higher frequencies in both modes.

3.2. Single-phase inverter stability analysis

Fig. 12 shows the single-phase DC-AC inverter controller uses a closed-loop system to regulate the output voltage V_{out} through the comparison between $V_{DC,ref}$ the reference voltage and actual voltage. The error signal passes through the PI controller G_{PI}^{INV} to control the inverter current I_{INV} through proportional gain K_p^{INV} and integral gain K_i^{INV}. The inverter controls its responses through the small-signal transfer function $(G_{INV}(s))$. This regulates its function to input and output condition alterations. The feedback mechanism in this control system guarantees steady voltage control along with consistent single-phase inverter operation.

Bode diagram in Fig. 13 demonstrates the performance of a single-phase inverter controller. The compensated system maintains a steady magnitude response while delivering an improved phase margin as compared to the uncompensated system. The compensated system achieves reduced phase lag thus ensuring better stability and frequency

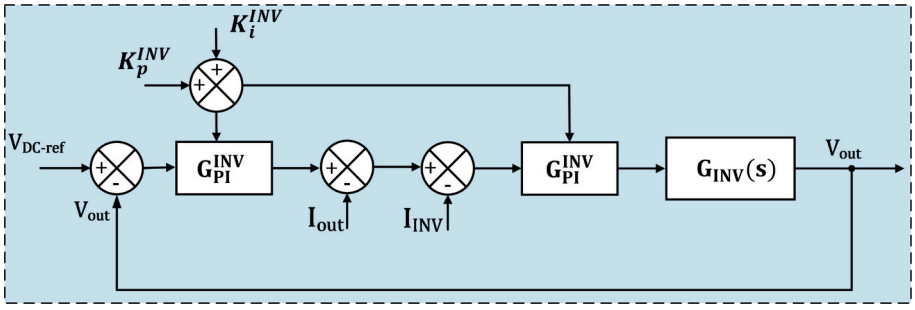

Fig. 12. Block diagram of closed loop single-phase inverter controller.

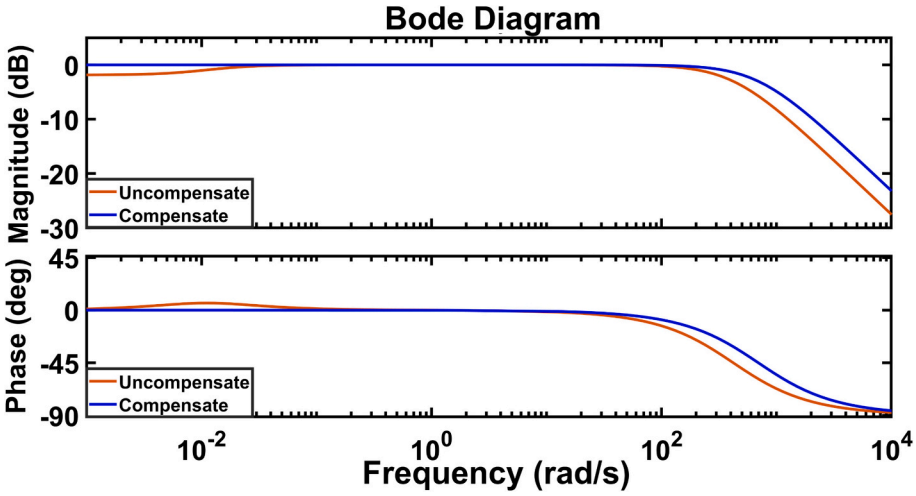

Fig. 13. Bode diagram of single-phase inverter controller.

response control at high frequencies for improved inverter performance.

3.3. HESPMS stability analysis

The stability analysis of the HESPMS is conducted through frequency-domain and time-domain evaluations. The study compares HESPMS performance against systems from [17,19,22,26] in frequency response and [17,19,24,26] for transient response evaluation which showcases HESPMS's fast response and low overshoot alongside high reliability in dynamic scenarios.

The stability analysis of the HESPMS is based on its transfer function:

$$G_{HESPMS}(s) = \frac{8.64s + 86.4672}{3.33 \times 10^{-2}(s + 10.427)(s + 2.49 \times 10^{2})} \quad (22)$$

In Fig. 14 the developed HESPMS shows superior performance when compared to the systems reported in previous studies. In terms of magnitude, HESPMS maintains a flat response at 0 dB up to $10^{-2} rad/s$, demonstrating minimal attenuation at low frequencies. In contrast, the system [22] starts to decline around 10^{1} rad/s, [19] after 10^{1} rad/s, and system [26] begins a similar decline at 10^{1} rad/s, with all systems experiencing a steeper fall in magnitude at higher frequencies. Specifically, HESPMS has a more gradual magnitude drop, especially beyond 10^{2} rad/s, whereas [22] exhibits a sharper drop and quicker attenuation past the same frequency.

The phase response of the proposed HESPMS begins at 0° degrees before transforming into -90° degrees while displaying low-pass filter characteristics. The other systems exhibit phase shifts that progress toward -90° degrees at frequencies near 10^{2} rad/s (for [19,22]) but create sharper transitions when compared to HESPMS. Lastly, [22] stabilizes at -90° rapidly along with HESPMS, while the phase shift in [17,26] is similarly smoother but occurs at higher frequencies.

In Fig. 15 HESPMS shows a settling time of approximately 0.03 s, with no significant overshoot. The rapid response and absence of oscillations show that HESPMS reaches its steady-state value without significant deviation thus proving excellent transient characteristics and stability. In comparison, the system from [24] exhibits a settling time of 0.25 to 0.3 s and an overshoot of 5 %. The system achieves stability between 0.5 and 0.6 s as it maintains an overshoot at 10 % according to [19]. The system needs between 0.45 and 0.5 s according to [26] to reach the settling time at 7 % overshoot although [17] achieves the settling time between 0.5 and 0.6 s with 3 % overshoot. These compared systems demonstrate slower stabilization and larger oscillations, leading to prolonged settling times and potential instability in dynamic conditions.

Overall, HESPMS outperforms other systems by offering smoother, more consistent responses across the frequency range, with lower attenuation and more gradual phase transitions. Also, the proposed HESPMS achieves faster settling times and minimal overshoot, making it a more efficient and reliable choice for applications requiring rapid stabilization and robust performance under dynamic disturbances.

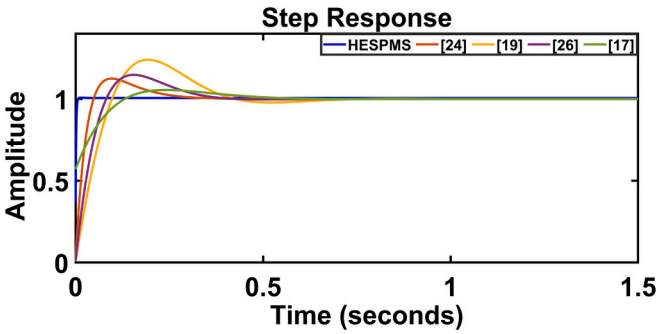

Fig. 15. Step response comparison between the proposed HESPMS and existing systems.

4. Proposed grid-isolated DC MG system

Fig. 16 illustrates the proposed grid-isolated MG system, which incorporates a PV array alongside a HESS consisting of a battery and SC to supply power for residential and EV charging loads.

The fuzzy logic-based MPPT controller assures optimal utilization of PV energy. The DC-DC boost converter regulates the voltage from the previous stage to connect to a 48 V DC bus. The propsed system enables an uninterrupted operation by controlling the distribution of power in various scenarios. The battery soothes out long-term power fluctuations, while the SC oversees transient fluctuations and high-frequency fluctuations to provide a quick response against sudden changes in load and to reduce further stress on the system. The HESS is coupled with a bi-directional converter to be able to manage the flow of energy effectively. The residential loads are powered by the DC bus through a DC-AC inverter, which incorporates an LC filter to produce pure sinusoidal AC, and the DC-DC converter delivers power to the EV charging load at the same time. Thus, effectively managing the dynamic loads of the system. This architecture ensures efficient power distribution by integrating renewable generation, energy storage, and flexible load management.

Table 4 presents the specifications for a proposed MG system by listing PV voltage, current, power, battery ratings and other system component specifications together with their respective values and units.

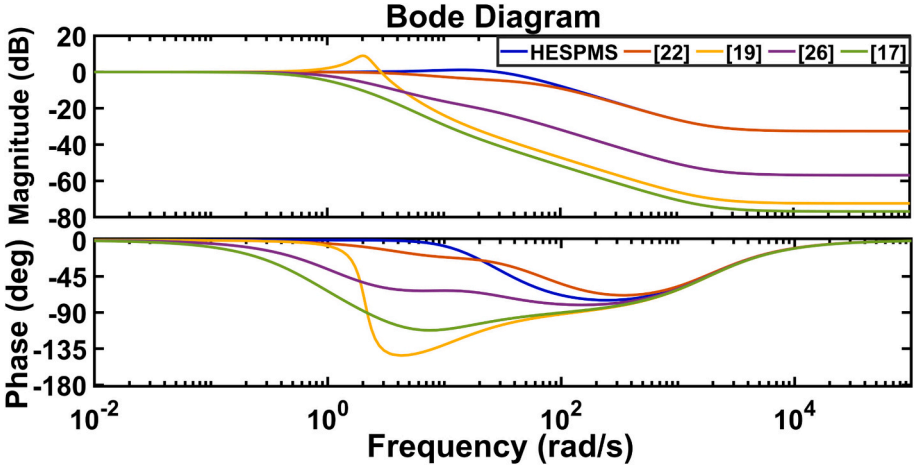

Fig. 14. Bode plot comparison between the proposed HESPMS and existing systems.

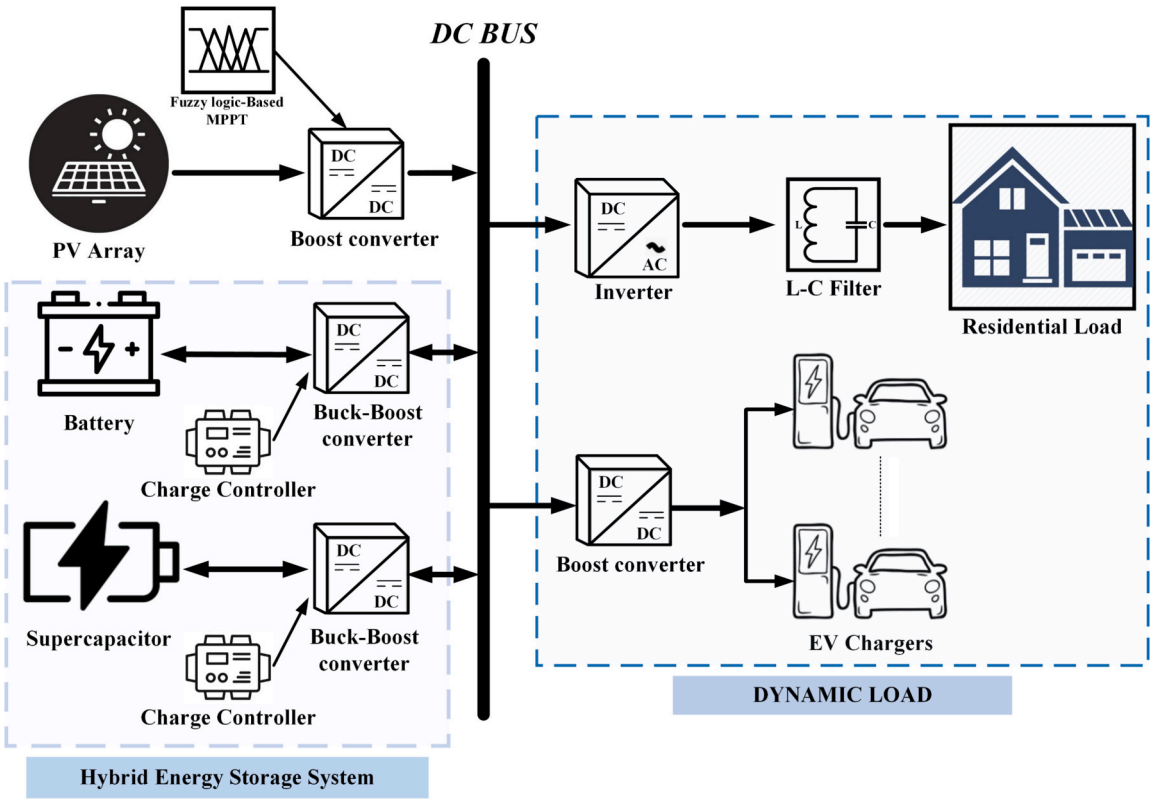

Fig. 16. Block diagram of the proposed grid-isolated DC MG System.

Table 4
Specifications of parameters of proposed MG System.

S. no	Description	Values	Unit
1	PV voltage	38	V
	PV current	7.35	A
	PV maximum power	6400	W
	Battery voltage	24	V
	Battery rating	200	Ah
2	SoC	15–95	%
	Nominal discharge current	86.85	A
	SC voltage	48	V
3	SC capacitance	1250	F
	SoC	20–90	%
4	Residential Constant load	1700	W
	Residential Varying load	0∼2500	W
5	EV Constant Load	1200	W
	EV Varying Load	0∼2400	W
6	Battery converter inductor	0.459	mH
	Battery converter capacitor	0.015	F
	SC converter inductor	0.459	mH
7	SC converter capacitor	0.020	F
	Switching frequency	10	kHz
8	Battery current controller gain	K_p^{Bat}=0.0169, K_i^{Bat}=0.1763	–
	SC current controller gain	K_p^{SC}=0.0169, K_i^{SC}=0.1763	–
9	PV Boost converter inductor	0.2996	mH
	PV Boost converter capacitor	0.649	F
	Switching frequency	10	kHz
10	DC bus voltage controller gain	K_p^{Bus}=0.1493, K_i^{Bus}=0.1783	–
11	DC bus voltage	48	V

4.1. Operational modes of the proposed grid-isolated DC MG system

Fig. 17 flowchart presents an outline of the power management framework for the proposed grid-isolated MG system. This process will begin with the measurement of key power variables of the system, such as PV generation (P_{PV}), battery power (P_{Bat}), SC power (P_{SC}), total generated power (P_{Gen}), and load demand (P_{Load}). The system also monitors the SoC limits for the battery and SC to maintain their operational ranges ensuring the safety of the storage devices.

During the first operation, when PV power is more than the load demand ($P_{PV} > P_{Load}$) the excess power mode is activated. This permits the stored excess energy, represented as P_{Excess}, within the battery and SC to work with maximum efficiency in terms of energy utilization. When power generation is not adequate to meet load demands ($P_{Gen} < P_{Load}$), the system checks the availability of ESS in order to mitigate the deficiency state. In this second case, when both energy storage units are available, the shortage, hereafter called $P_{Deficit}$, is supplied by discharging the battery. On the other hand, in the third case, if there is only an SC storage unit in operation, that unit will discharge to meet the shortfall, represented by $P_{Bat.Discharge} = P_{Defecit}$ or $P_{SC.Discharge} = P_{Defecit}$. In the last scenario, both the PV system and the storage units are unable to meet the total load demand. Thus, load shedding is executed which leads to the total load being disconnected ($P_{Load} = 0$) to ensure the system's stability. This framework ensures energy management is carried out systematically and efficiently due to its ability to change power generation, and demand in a way that maintains operational stability, regardless of changes in conditions.

4.2. Energy management strategy algorithm for the proposed HESPMS

The objective of this power management algorithm is to achieve optimized energy flow to maintain a proper balance between supply and demand for different operational modes. Four specific case studies have been shown below, each of the cases represents a distinct operational state of the proposed system.

4.2.1. Case 1: surplus energy generation and HESS charging

In this scenario, the power generated by the PV system (P_{PV}) exceeds the total load demand. The total load (P_{Load}) consists of the EV load (P_{EV}) and the residential load (P_{RL}).

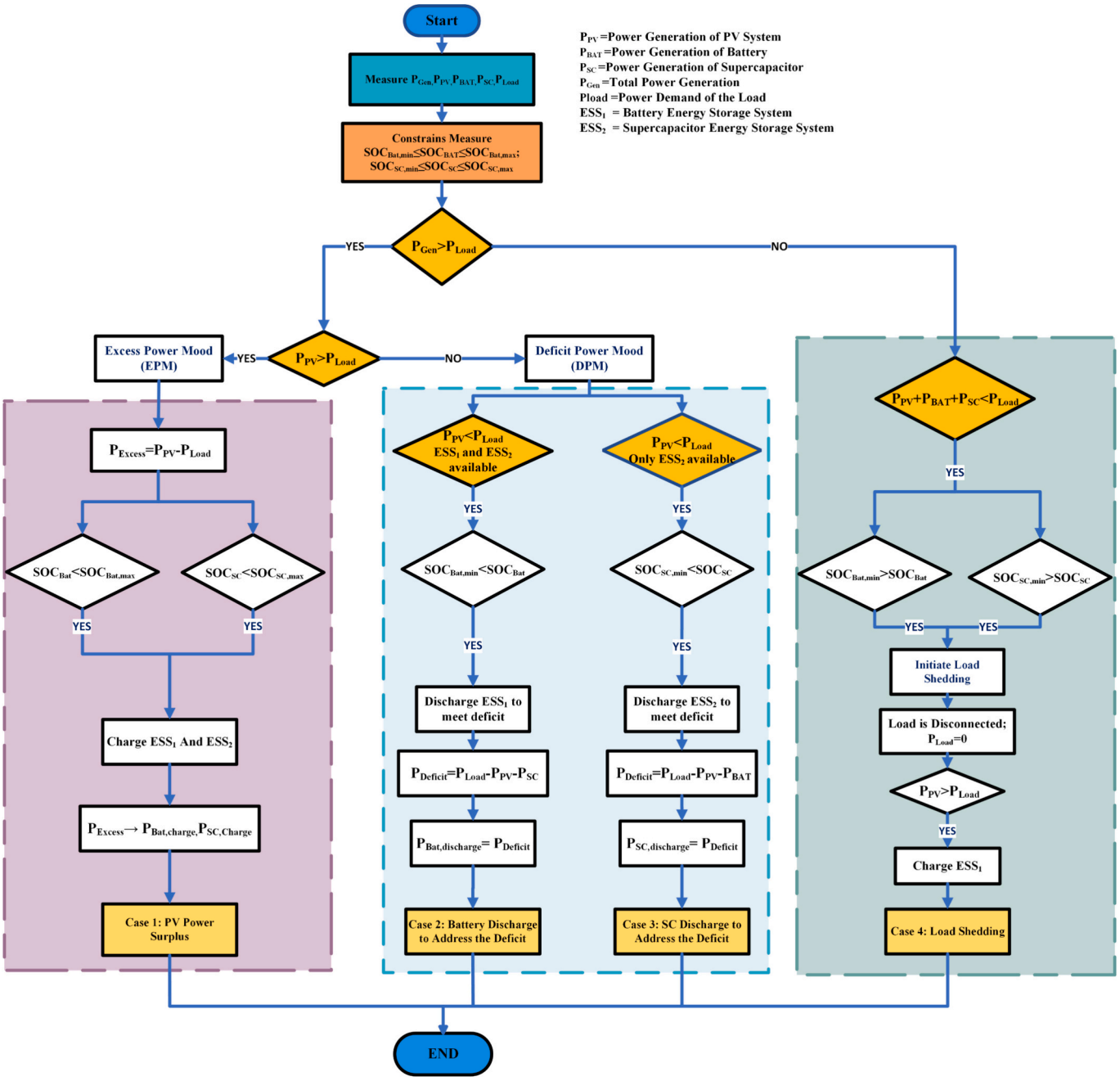

Fig. 17. Flowchart of the energy management strategy algorithm of the proposed system.

The power generated by the PV system:

$$P_{PV} = V_{PV} \times I_{PV} \tag{23}$$

Here, V_{PV} and I_{PV} is the voltage and current generated by the PV system respectively.

Total generated power including the HESS:

$$P_{Gen} = P_{PV} + P_{Bat} + P_{SC} \tag{24}$$

In Eq. (24) P_{Bat} and P_{SC} represent the power produced by the battery and SC, respectively.

The load demand which considers residential loads and multiple EVs:

$$P_{Load} = P_{RL} + \sum_{j=1}^{N_{EV}} P_{EV} \tag{25}$$

Here, in Eq. (25) P_{RL} is the power consumption of the residential load, N_{EV} is the number of EV chargers, P_{EV} is the power consumption of the EV charging load.

As the generation of PV power surplus, the total load demand:

$$P_{PV} > P_{Load} \rightarrow P_{Gen} > P_{Load} \tag{26}$$

The available excess power P_{Excess} is:

$$P_{Excess} = P_{PV} - P_{Load} \tag{27}$$

The excess power is utilized by This excess power is utilized to charge both the battery and the SC.

$$P_{Excess} = P_{Bat,chg} + P_{SC,chg} \tag{28}$$

As charging, the power flows into the battery and SC, so the power contributions P_{Bat} and P_{SC} are negative. Thus,

$$P_{Bat} = -P_{Bat,chg} \ (\text{With } P_{Bat,chg} > 0) \tag{29}$$

$$P_{SC} = -P_{SC,chg} \ (\text{With } P_{SC,chg} > 0) \tag{30}$$

The overall power balance in this system:

$$P_{PV} = P_{Load} + P_{Bat,chg} + P_{SC,chg} \tag{31}$$

This is the operational range within which the SoC is required to operate.

$$\text{Battery SoC Constraints} : SoC_{Bat}^{min} \leq SoC_{Bat} \leq SoC_{Bat}^{max} \tag{32}$$

$$\text{SC SoC Constraints} : SoC_{SC}^{min} \leq SoC_{SC} \leq SoC_{SC}^{max} \tag{33}$$

Here, SoC_{Bat}^{min} and SoC_{Bat}^{max} are the minimum and maximum SoC for the battery. SoC_{SC}^{min} and SoC_{SC}^{max} are the minimum and maximum SoC for the SC. This Eqs. (32) and (33) prevent the HESS from over-discharge or overcharge.

Charging transpires under the following conditions:

$$\text{For the Battery} : \begin{cases} P_{Bat,chg} > 0 \\ SoC_{Bat} < SOC_{Bat}^{max} \end{cases} \tag{34}$$

$$\text{For the SC} : \begin{cases} P_{SC,chg} > 0 \\ SoC_{SC} < SoC_{SC}^{max} \end{cases} \tag{35}$$

This Eqs. (34) and (35) assure that charging occurs solely when there is available capacity in the storage devices.

The objective of the HESPMS is to optimize energy flow by balancing supply and demand. This is done by minimizing the squared difference between PV generation, load demand, and the charging power of the battery and SC over the time period $[t_{initial}, t_{final}]$. Mathematically, this is expressed as:

$$min\left\{ \int_{t_{initial}}^{t_{final}} \left[P_{PV} - P_{Load} - P_{Bat} - P_{SC}\right]^2 dt \right\} \tag{36}$$

4.2.2. Case 2: power shortfall with battery discharge

In this scenario, the power generated by the PV system (P_{PV}) is insufficient to meet the total load demand. As a result, the battery discharges to supply the additional power required by the load. Thus,

$$P_{PV} < P_{Load} \tag{37}$$

The deficit power required from the battery is:

$$P_{Deficit} = P_{Load} - P_{PV} \tag{38}$$

The deficit power is compensated by discharging the battery,

$$P_{Deficit} = P_{Bat,dis} \tag{39}$$

The overall power balance in the system during the power shortfall is:

$$P_{PV} + P_{Bat,dis} + P_{SC,dis} = P_{Load} \tag{40}$$

The operational range of HESS, within which the SoC is required to operate is given in Eqs. (32) and (33).

For this case, the battery discharges under the following conditions, and upon reaching this threshold, discharging ceases to prevent damage:

$$\begin{cases} P_{Bat,dis} > 0, if\ SoC_{Bat} > SoC_{Bat}^{min} \\ P_{Bat,dis} = 0, if\ SoC_{Bat} \leq SoC_{Bat}^{min} \end{cases} \tag{41}$$

The objective of the HESPMS is to minimize the power shortfall by efficiently utilizing the stored energy of the battery. This is accomplished by minimizing the squared deviation between the load demand and the aggregate power from the PV system, the SC, and the discharging battery, over the specified time interval $[t_{initial}, t_{final}]$. Mathematically, this is expressed as:

$$min\left\{ \int_{t_{initial}}^{t_{final}} \left[P_{Load} - \left(P_{PV} + P_{SC,dis} + P_{Bat,dis}\right)\right]^2 dt \right\} \tag{42}$$

4.2.3. Case 3: power shortfall with SC discharge

In this scenario, the power generated by the PV system (P_{PV}) and the battery (P_{Bat}) is insufficient to meet the total load demand. As a result, the SC discharges to supply the additional power required by the load. Thus, the condition,

$$P_{PV} + P_{Bat} < P_{Load} \tag{43}$$

The deficit power required from the battery is:

$$P_{Deficit} = P_{Load} - (P_{PV} + P_{Bat}) \tag{44}$$

The deficit power is compensated by discharging the SC,

$$P_{Deficit} = P_{SC,dis} \tag{45}$$

The overall power balance in the system during the power shortfall is:

$$P_{PV} + P_{Bat} + P_{SC,dis} = P_{Load} \tag{46}$$

The operational range of HESS, within which the SoC is required to operate is given in Eqs. (32) and (33).

For this case, the SC discharges under the following conditions, and upon reaching this threshold, discharging ceases to prevent damage:

$$\begin{cases} P_{SC,dis} > 0, if\ SoC_{SC} > SoC_{SC}^{min} \\ P_{SC,dis} = 0, if\ SoC_{SC} \leq SoC_{SC}^{min} \end{cases} \tag{47}$$

The objective of the HESPMS is to minimize the power shortfall by efficiently utilizing the stored energy of the SC. This is accomplished by reducing the squared deviation between the load demand and total power from the PV system, the battery, and the discharging SC, during the specified time $[t_{initial}, t_{final}]$. Mathematically, this is expressed as:

$$min\left\{ \int_{t_{initial}}^{t_{final}} \left[P_{Load} - \left(P_{PV} + P_{Bat} + P_{SC,dis}\right)\right]^2 dt \right\} \tag{48}$$

4.2.4. Case 4: power shortfall leading to load shedding

In this scenario, the PV system (P_{PV}), battery (P_{Bat}), and SC (P_{SC}) cannot meet the total load demand. Thus, load shedding mode is employed to mitigate the power imbalance. The objective of the power management plan is to optimize system energy distribution by minimizing the sum of total load demand. This will, therefore, ensure protection against overloading and instability during shortage periods. This condition is expressed by:

$$P_{PV} + P_{Bat} + P_{SC} < P_{Load}; Hence, P_{Gen} < P_{Load} \tag{49}$$

Additionally, the SoC for both the battery and the SC are below their minimum thresholds:

$$\begin{cases} SoC_{Bat,min} > SoC_{Bat} \\ SoC_{SC,min} > SoC_{SC} \end{cases} \tag{50}$$

Due to the power shortfall, the total load is disconnected, and initiate the load shedding:

$$P_{Load} = 0 \tag{51}$$

The system enters load-shedding mode and remains in this state until PV power is sufficient to satisfy the load demand. After exiting load-shedding mode, the HESPMS seeks to optimize the use of available PV power for battery charging while satisfying load demand. Excess power remaining after the load supply is directed toward battery charging, while the inactive SC sustains power balance without necessitating

power transmission. Thus:

$$\begin{cases} P_{PV} > P_{Load} \\ P_{PV} = -P_{Bat,chg} \\ P_{SC} = 0 \end{cases} \quad (52)$$

The power balance equation:

$$P_{PV} + P_{Bat} + P_{SC} = P_{Load} \quad (53)$$

Since, the $P_{PV} > P_{Load}$ and $P_{SC} = 0$, and considering $P_{Bat} = -P_{Bat,chg}$

$$P_{PV} - P_{Bat,chg} = 0 \quad (54)$$

Hence, Eq. (54) confirms that all PV power is used to charge the battery.

The operational range of HESS, within which the SoC is required to operate is given in Eqs. (32) and (33).

The primary objective of the HESPMS is to maximize the utilization of available PV power for battery charging after load shedding. This is achieved by maximizing the integral of the charging power of the battery, using the available PV power over the time $[t_{initial}, t_{final}]$. Mathematically, this is expressed as:

$$max_{P_{Bat,chg}} \left\{ \int_{t_{initial}}^{t_{final}} P_{Bat,chg} dt \right\} \quad (55)$$

5. Results and discussion

The proposed system is assessed using the grid-isolated MG with a HESS and dynamic loads comprised of residential consumption and EV charging load as illustrated in Fig. 16. The proposed system is simulated in MATLAB/Simulink operating under four scenarios, each operating for 4 s. Four operating modes with varying generation and load demands are simulated to assess the effectiveness and reliability of the proposed HESPMS during rapid changes in operating conditions.

5.1. Case 1: surplus energy generation and HESS charging

The PV system generated a surplus of power, exceeding the total load demand in this scenario. In Fig. 18 (h), from 0 to 1 s, the PV power reached approximately 3800 W, and the loads remained at around 1700 W for the residential load and 1200 W for the EV load. Both the residential and EV load demands are fully met by the PV power generation. Meanwhile, the battery was charging at a rate of −900 W. The SoC profiles of the HES are shown in Fig. 18 (e) and (f). Between 1 and 2 s, the PV power increased to 4500 W, whereas the EV load increased to 2400 W, with the residential load remaining at 1700 W. The battery is charging at a rate of −400 W. Within 2 to 3 s, the EV load decreased to 1200 W, while the residential load increased to 2600 W. Simultaneously, the PV power generation increased to 5100 W. From 3 to 4 s, the residential load decreased to 1700 W, maintaining the EV load at 1200 W, and the PV power further increased to 6400 W. Under transient conditions, the SC contributes to stability and alleviates the stress on the battery.

Fig. 18 (a) shows the solar irradiation graph. Fig. 18 (b) illustrates the PV voltage and current, while Fig. 18 (c) shows the DC link voltage, which remains stable and smooth throughout the entire period, exhibiting only minor spikes that confirm the system stability. Fig. 18 (d) demonstrates smooth sinusoidal output confirming the stability and adaptability of the inverter to varying HESS. Total Harmonic Distortion (THD) values of the inverter output in the proposed system are shown in Fig. 18 (g), which shows that the THD is 2.13 % for voltage and 2.34 % for current. These values are less than the IEEE standard limit of 5 % to confirm the acceptable power quality of the system.

5.2. Case 2: power shortfall with battery discharge

The power produced by the PV system is insufficient to fulfill the total load demands in this scenario. The battery storage discharges to provide the additional power needed by the load, while the SC enhances stability and reduces stress on the battery during this time. Fig. 19 (h) illustrate that from 0 to 1 s, the PV output power is approximately 2500 W, which is insufficient to meet the total load demand. Therefore, this power deficit of 400 W was compensated by discharging the battery to balance the power. During this time, SC stabilizes the system by providing transient power for a short period of time. Between 1 and 2 s, the PV power decreased to 1800 W, the EV load demand increased to 2400 W, and the residential load remained at 1700 W. To fill the gap, the battery started discharging at 2300 W. Between 2 and 3 s, the PV power decreased to 1200 W, whereas the residential and EV loads were at 2600 W and 1200 W, respectively. The battery discharge rate increased to 2600 W to address the power deficit. Between 3 and 4 s, the irradiation is minimal with a PV power of 600 W, corresponding to the residential load of 1700 W, and the EV load of 1200 W, Thus, the battery discharging at 2300 W to meet the deficit.

In Fig. 19 (e) and (f) illustrate the SoC of the HES in this mode. Fig. 19 (c) illustrates the DC link voltage, which exhibited only minor spikes during transient conditions, thereby confirming system stability. Fig. 19 (a) shows the solar irradiation graph. Fig. 19 (b) shows the PV voltage and current output. Fig. 19 (d) illustrates the MG inverter voltage and current characteristics, showing smooth sinusoidal waveforms that validate the inverter stability and adaptability. THD values of the inverter output of the proposed system are shown in Fig. 19 (g), which shows that the THD is 2.03 % and 2.05 % for voltage and current, respectively. The values are well below the threshold of 5 % according to the IEEE standard for acceptable power quality.

5.3. Case 3: power shortfall with SC discharge

The power generated by the PV system and the battery falls short of meeting the total load requirements in this scenario. The SC discharges to supply additional power required by the load. In Fig. 20 (h), from 0 to 1 s, 2500 W of PV power was produced, and the residential and EV loads were 1700 W and 1200 W, respectively. The battery provided the remaining 300 W to fill the power gap. Between 1 and 2 s, the residential load demand rises to 2600 W, the EV load remains at 1200 W, and the PV power falls to 1100 W. In this period, the load demand surpasses the total capacity of the PV system while the battery reaches its minimum SoC limit. To maintain a steady power supply, the SC began supplying 2700 W. This results in a brief spike in the DC link voltage that stabilizes within a few milliseconds, as seen in Fig. 20 (c). Between 2 and 3 s, the PV power generation decreased to 600 W, the residential load dropped to 1700 W, and the EV load increased to 2400 W. The SC compensates for this by providing 3500 W. Then, from 3 to 4 s, the PV power decreased to 150 W, whereas the residential and EV loads decreased to 1700 W and 1200 W, respectively. During this period, the SC supplied 2750 W to balance the load demand, acting as the primary backup power source.

Fig. 20 (f) illustrates the SoC of the SC during the discharging mode between 1 and 4 s. When the minimum SoC threshold for the battery was reached at 1 s, the battery was disconnected from the system, as indicated in Fig. 20 (e). Fig. 20 (a) shows the solar irradiation graph. Fig. 20 (b) displays the PV voltage and current, whereas Fig. 20 (c) demonstrates the stability of the DC-link voltage. Fig. 20 (d) illustrates the MG inverter voltage and current characteristics, showing smooth sinusoidal waveforms that validate the system's stability and adaptability. In THD values of the inverter output of the proposed system are shown in Fig. 20 (g), which shows that the THD is 2.61 % and 2.73 % for voltage and current, respectively. The values are well below the threshold of 5 % according to the IEEE standard for acceptable power quality.

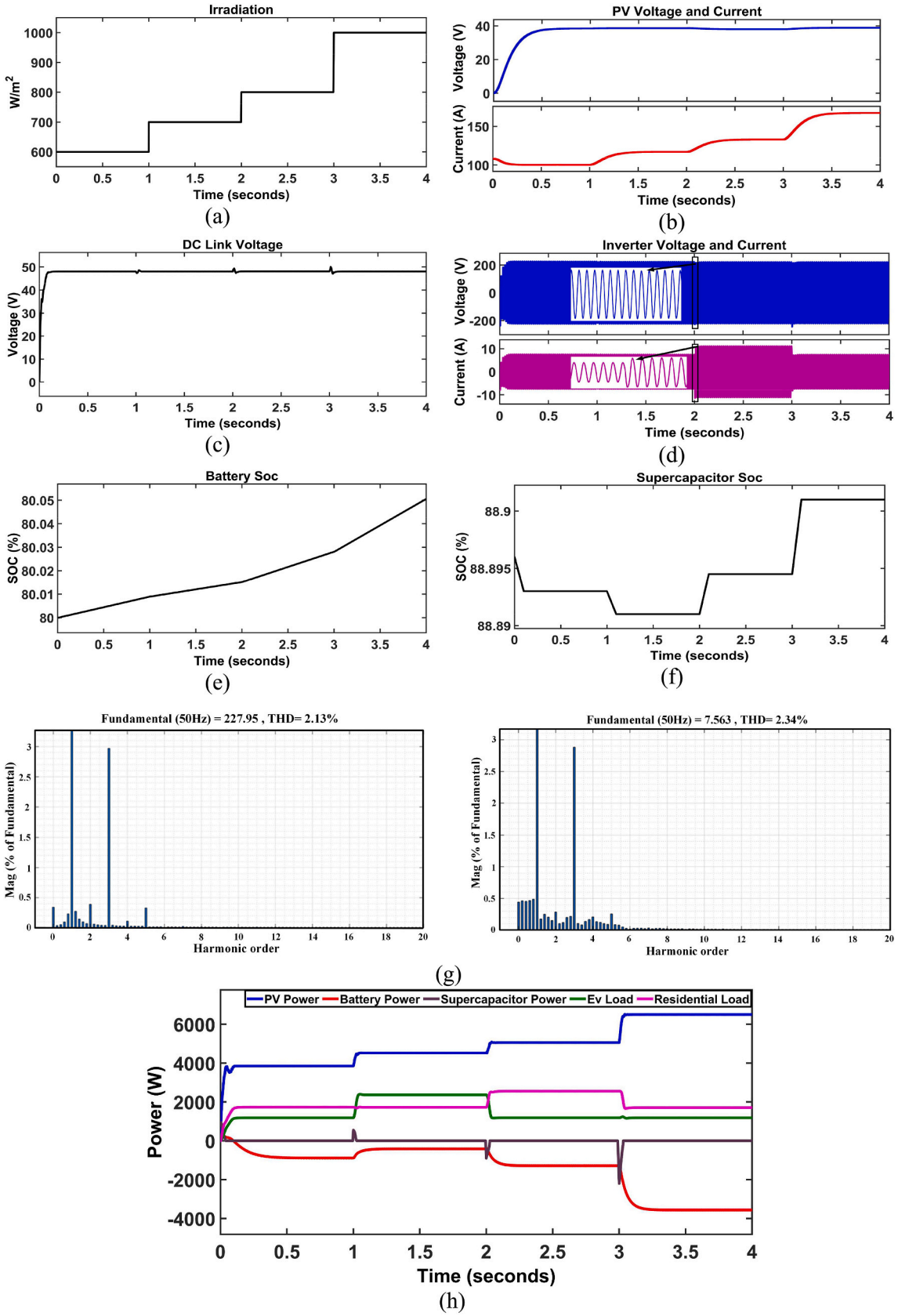

Fig. 18. (a) Solar irradiation, (b) PV voltage and current, (c) DC link voltage, (d) Inverter voltage and current, (e) Battery SoC, (f) SC SoC, (g) THD of inverter's output voltage and output current, (h) Power management profile.

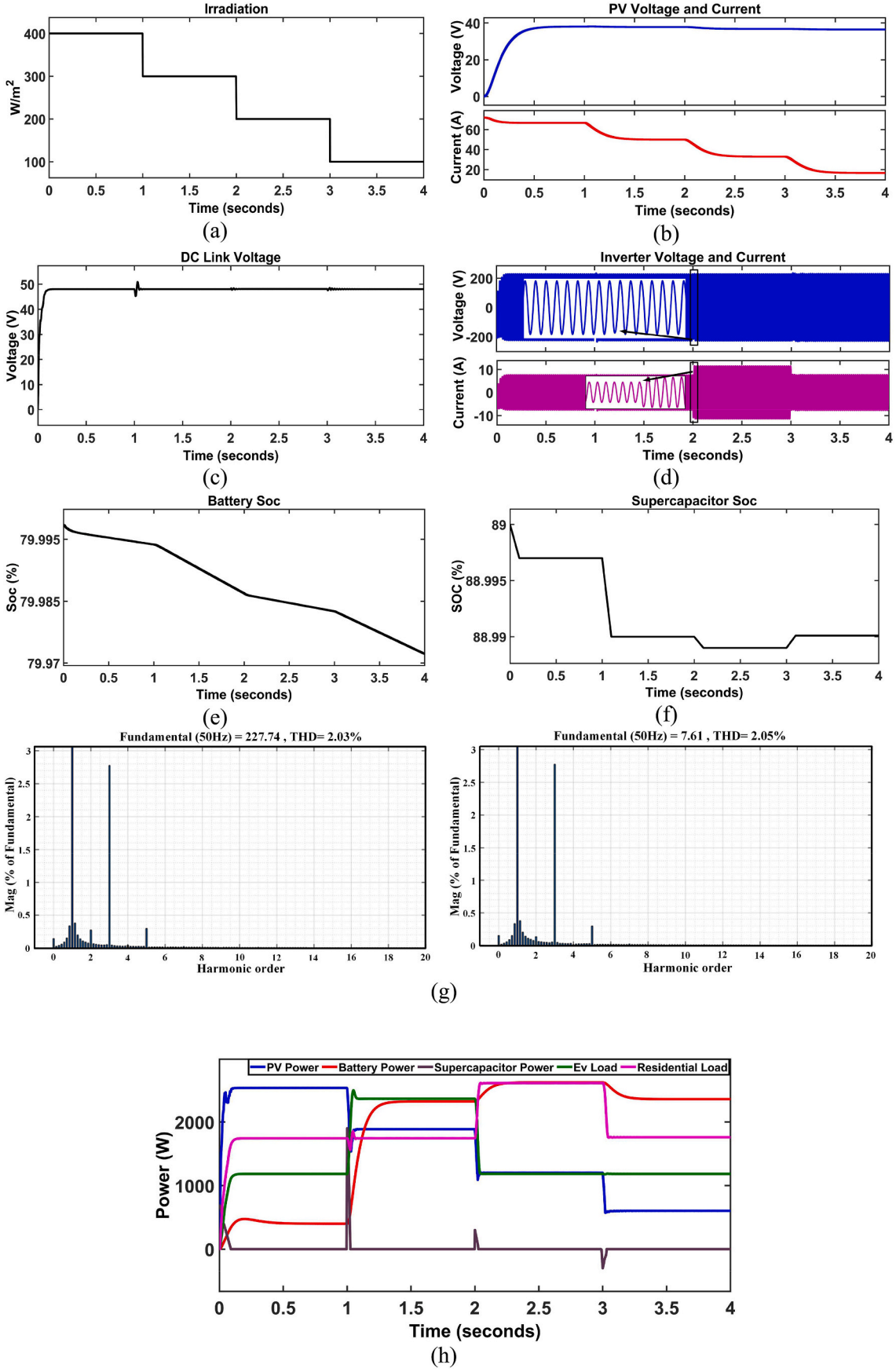

Fig. 19. (a) Solar irradiation, (b) PV voltage and current, (c) DC link voltage, (d) Inverter voltage and current, (e) Battery SoC, (f) SC SoC, (g) THD of inverter's output voltage and output current, (h) Power management Profile.

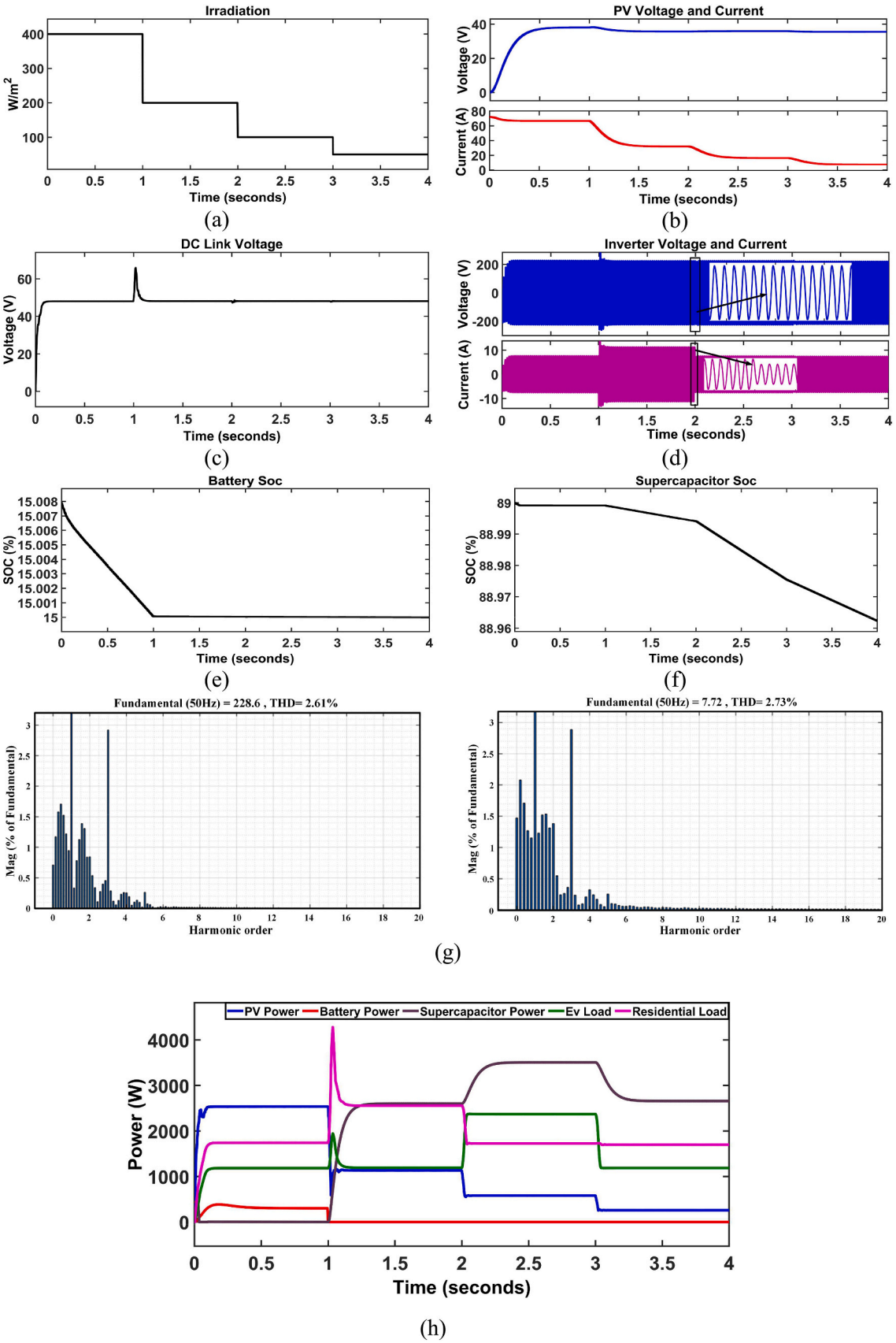

Fig. 20. (a) Solar irradiation, (b) PV voltage and current, (c) DC link voltage, (d) Inverter voltage and current, (e) Battery SoC, (f) SC SoC, (g) THD of inverter's output voltage and output current, (h) Power management profile.

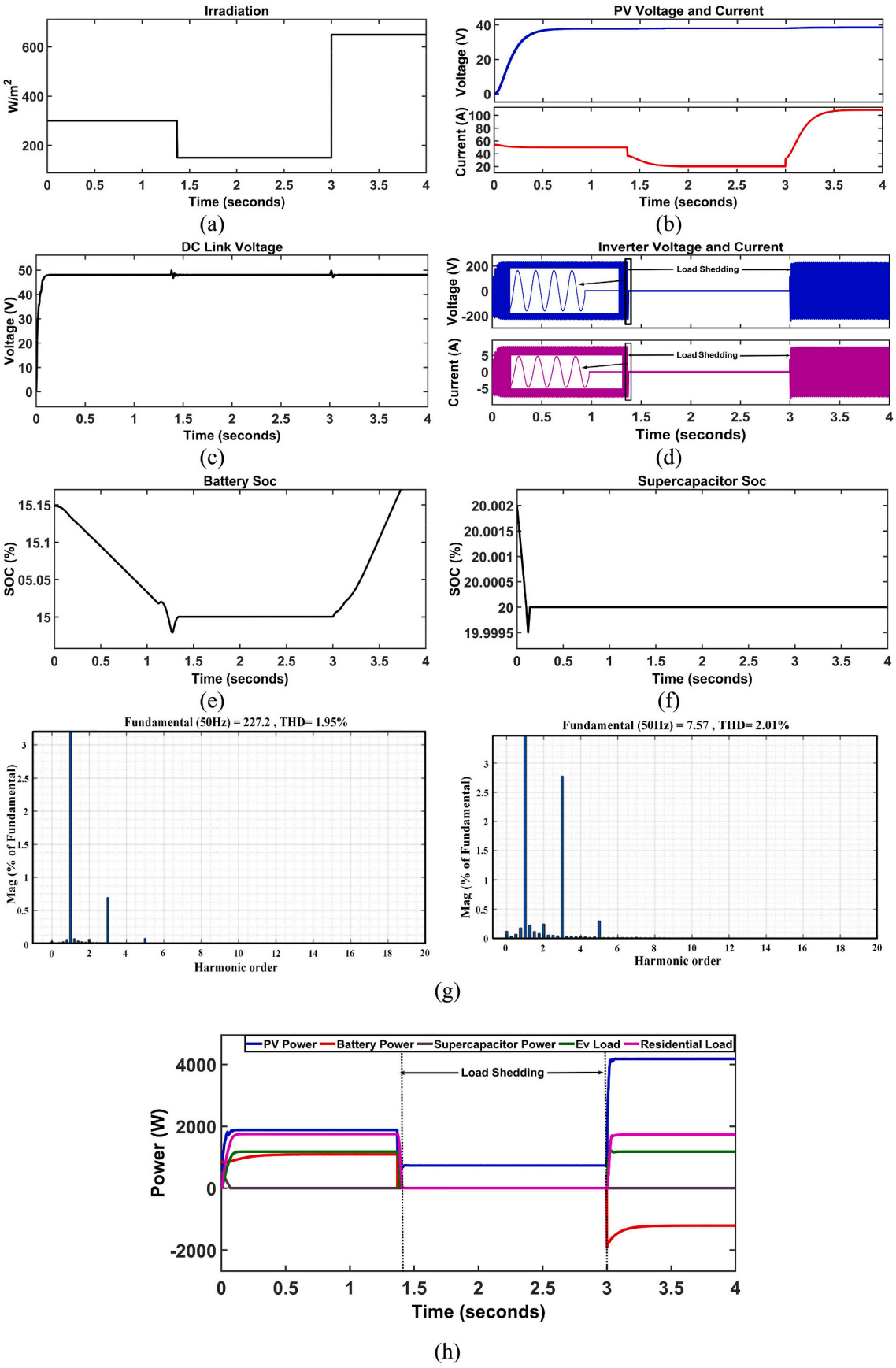

Fig. 21. (a) Solar irradiation, (b) PV voltage and current, (c) DC link voltage, (d) Inverter voltage and current, (e) Battery SoC, (f) SC SoC, (g) THD of inverter's output voltage and output current, (h) Power management profile.

5.4. Case 4: power shortfall leading to load shedding

The PV system, battery, and SC are insufficient to fulfill the total load demand in this scenario, necessitating load shedding to mitigate the power imbalance. The HESPMS optimizes energy distribution by minimizing load demand and providing protection against overloads and instability during power shortages. Fig. 21 (h) illustrates the power management profile for the operation. In Fig. 21 (h), from 0 to 1.37 s, the PV system provides a steady output of 1850 W, the residential load was 1700 W, and the EV load demand was 1200 W. The battery supplies the 1050 W to fulfill deficit. Between 1.37 and 3 s, the PV power decreases to 800 W, which fails to meet the total load demands. The battery reaches the minimum SoC threshold at 1.37 s and SC also discharged upon reaching the minimum SoC threshold at 0.1 s, as shown in Fig. 21 (e) and (f). Thus, load shedding is initiated. Both residential and EV loads are disconnected to prevent further discharge and potential instability. During this period, the MG inverter was shut down, as illustrated in Fig. 21 (d). Fig. 21 (h) shows, that between 3 and 4 s, the PV output increases to 4100 W. This increased generation allows the system to fully supply the residential load of 1700 W and EV load of 1200 W. With sufficient PV power, load shedding was deactivated, and the battery was reconnected. The surplus PV power charges the battery at a rate of −1200 W. The system manages power fluctuations through load shedding and enables a return to normal operation when power generation meets demand.

During this scenario, as illustrated in Fig. 21 (c), the DC link voltage consistently maintained a value of 48 V, thereby validating the system's stability. Fig. 21 (a) shows the solar irradiation graph. Fig. 21 (b) displays the PV voltage and current. The THD analysis of the system inverter's output, shown in Fig. 21 (g), indicates voltage and current values are at 1.95 % and 2.01 %, well below the IEEE 5 % threshold for acceptable power quality. Table 5 shows the power flow response to changes in irradiation and load for the proposed system, detailing the interaction between the PV system, battery, SC, and loads across four cases. It also presents the corresponding SoC state for the battery and SC.

6. Comparative analysis

6.1. Comparison of the proposed HESPMS with the existing studies

In this section, the proposed HESPMS is compared with the existing studies documented in the literature. The comparison was carried out based on the following critical factors: DC bus voltage, dynamic load capability, EV charger integration, power management strategy, and load-shedding mode. By analyzing each of these aspects, we demonstrate that our proposed HESPMS exhibits superior performance and effectiveness compared to the existing system. Table 6 details the advantages of the proposed technique concerning the primary challenges encountered in energy system management.

6.2. Proposed FLC-based MPPT and conventional MPPT controller comparison

Here, Table 7 presents a quantitative comparison between the proposed fuzzy logic-based MPPT control and conventional MPPT control methods. The focus of the analysis is mainly on three important

Table 5
Power flow response to variations in irradiation and load of the proposed system.

Duration (s)	Irradiation (W/m^2)	PV (W)	Battery (W)	SC (W)	Residential load (W)	EV load (W)	SoC_{SC}	SoC_{Bat}
				Case 1				
0–1	600	3800	−900	1050($t_{0s–0.02s}$)	1700	1200	D($t_{0s–0.02s}$)	C
1–2	700	4500	−400	500($t_{1s–1.02s}$)	1700	2400	D($t_{1s–1.01s}$)	C
2–3	800	5100	−1300	−900($t_{2s–2.02s}$)	2600	1200	C($t_{2s–2.01s}$)	C
3–4	1000	6400	−3500	−2200($t_{3s–3.02s}$)	1700	1200	C($t_{3s–3.01s}$)	C
				Case 2				
0–1	400	2500	400	620($t_{0s–0.02s}$)	1700	1200	D($t_{0s–0.02s}$)	D
1–2	300	1800	2300	1900 ($t_{1s–1.02s}$)	1700	2400	D ($t_{1s–1.01s}$)	D
2–3	200	1200	2600	300($t_{2s–2.2s}$)	2600	1200	D($t_{2s–2.01s}$)	D
3–4	100	600	2360	−300($t_{3s–3.2s}$)	1700	1200	C($t_{3s–3.01s}$)	D
				Case 3				
0–1	400	2500	300	450($t_{0s–0.02s}$)	1700	1200	D($t_{0s–0.02s}$)	D
1–2	200	1100	0	2700	2600	1200	D	N/A
2–3	100	600	0	3500	1700	2400	D	N/A
3–4	40	150	0	2750	1700	1200	D	N/A
				Case 4				
0–1.37	300	1800	1050	700($t_{0–0.012s}$)	1700	1200	D($t_{0–0.012s}$)	D
1.37–3	150	800	0	0	0	0	N/A	N/A
3–4	650	4100	−1200	0	1700	1200	N/A	C

NB: Charging = C, Discharging = D

Table 6
Comparison between proposed HESPMS and existing DC MG systems.

Ref.	Authors	DC-bus voltage	Dynamic load capability	Power management strategy	EV charger integrated	Load shedding mode
[17]	P. Singh and J. Singh Lather (2021)	Stable	Available	Present	No	Not Provisioned
[19]	Arunkumar C.R. et al. (2022)	Stable	Unavailable	Present	No	Not Provisioned
[21]	S. Remache et al. (2022)	Noisy	Unavailable	Present	No	Not Provisioned
[22]	Punna, S et al. (2022)	Noisy	Unavailable	Absent	No	Not Provisioned
[24]	Suchismita Patel et al. (2023)	Stable	Unavailable	Present	No	Not Provisioned
[26]	Hassan A. et al. (2023)	Stable	Available	Present	No	Not Provisioned
	Proposed HESPMS	**Stable**	**Available**	**Present**	**Yes**	**Provisioned**

Table 7
Performance Comparison of Proposed fuzzy-logic-Based MPPT and Conventional MPPT Methods.

Ref.	[19]	[22]	[35]	[36]	Proposed
Voltage regulation (V_{Reg})	±0.14158	±0.26	±0.9	±0.13542	±0.046
Peak overshoot (P_{OS})	6.12 %	26 %	11 %	7.83 %	2.53 %
Settling time (t_{ss})	150 ms	100 ms	631 ms	290 ms	20 ms

performance measures: voltage regulation (V_{Reg}), peak overshoot (P_{OS}), and settling time (t_{ss}), which are vital for assessing the effectiveness and stability of MPPT algorithms. These indicators of performance are particularly significant for situations where dynamic environmental factors are involved, such as in PV systems.

The analysis used bus voltage variations during transitions to derive metric values which closely represent renewable energy system operational conditions. The evaluation analyzes tracking efficiency, response speed, and recovery capabilities during brief disturbances of MPPT method operations. The results from Table 7 demonstrate that the fuzzy logic-based MPPT controller achieves superior system stability and rapid response capabilities than traditional approaches under different system conditions (Fig. 22).

7. Conclusion

The proposed HESPMS achieved successful development and validation to deliver optimized power continuity alongside efficient resource management and enhanced stability for grid-isolated solar-powered DC MG system. The proposed system uses HESS together with an adaptive load management system which enables effective control of both battery and SC charge-discharge operations to maximize storage component lifespan while maintaining system performance across various operational conditions. Utilizing a fuzzy logic-based MPPT controller, the system effectively harnesses PV energy and stabilizes the DC link voltage. Key performance metrics include an average voltage regulation of ±0.046, peak overshoot of 2.53 %, and rapid settling time of 20 ms, all contributing to the system's outstanding stability and transient response. Four cases were discussed, with Case 1 demonstrating the system's effective use of PV energy during surplus conditions, where the SC and battery adeptly managed transients and maintained stable charging. During power shortfalls in Case 2, the battery supplied energy while the SC reduced strain by managing transients. Case 3 showcased the SC's quick response to load fluctuations, balancing supply and demand, Case 4 highlighted the system's resilience during power shortages. The adaptive load shedding was used to maintain stability and safeguard the DC link voltage in this case. The HESPMS controller achieves superior performance results across time and frequency domains. The frequency domain response of this

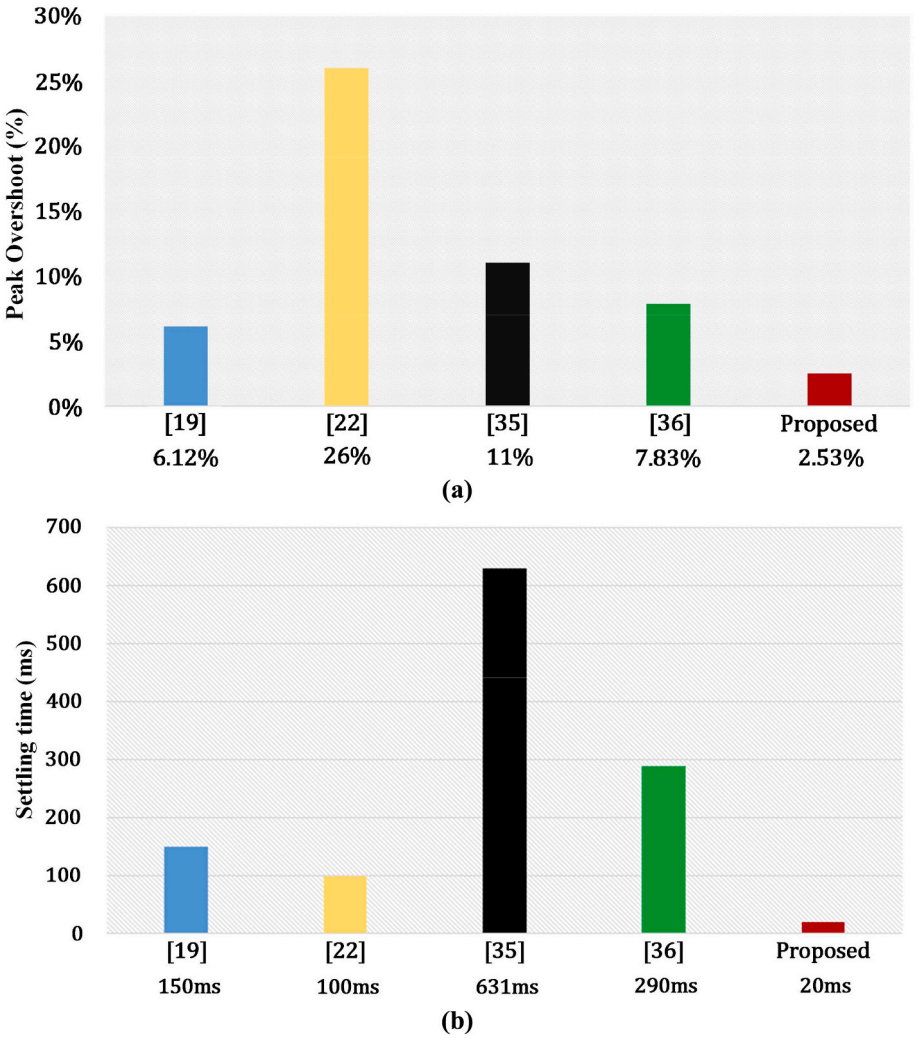

Fig. 22. Performance comparison of (a) peak overshoot and (b) settling time for proposed and conventional MPPT methods based on DC bus voltage.

controller shows a flat magnitude at 0 dB from 0 to 10^{-2} rad/s before it starts to attenuate. A stable low-pass filter behavior emerges from the phase response as it gradually shifts from 0° to −90°. Furthermore, the HESPMS controller achieves a settling time of 0.03 s in the time domain with no significant overshoot, indicating rapid stabilization along with superior transient performance. The controller demonstrates dependable and effective performance in dynamic applications through its optimal results obtained in both time and frequency domains. In conclusion, HESPMS provides a versatile and dependable power-management solution, ensuring consistent power continuity and robustness in fluctuating load conditions. This study establishes a solid basis for future developments in grid-isolated MGs, aiding in the continuous quest for sustainable and efficient energy systems.

The future development of HESPMS will focus on addressing operational barriers to boost system efficiency and expand its capabilities. The primary obstacle in RES integration involves wind and solar power systems because they introduce unpredictable power generation fluctuations. Another area of emphasis is enhancing AI-driven control strategies for load forecasting and real-time optimization. Also, the next initiatives will focus on refining these algorithms to address challenges like sensor data quality, communication delays, and real-time processing, ultimately leading to enhanced accuracy and responsiveness. Furthermore, the incorporation of HESSs into existing grid infrastructure presents challenges concerning system synchronization, stability, and compliance with regulatory standards. In the future, the proposed system's practical implementation will include tests to address potential challenges that may arise during execution. By tackling these challenges, our upcoming investigations will enhance HESPMS performance, scalability, and reliability, facilitating their seamless integration with renewable energy sources and current grid systems.

CRediT authorship contribution statement

Jahidul Islam Shuvo: Writing – review & editing, Writing – original draft, Validation, Software, Methodology, Investigation, Formal analysis, Data curation, Conceptualization. **Md. Badoruzzaman:** Writing – review & editing, Writing – original draft, Visualization, Validation, Software, Methodology, Conceptualization, Formal analysis. **Shaikh Tawhidul Islam Anik:** Writing – original draft, Methodology, Investigation, Formal analysis, Data curation, Conceptualization, Software. **Shameem Ahmad:** Writing – review & editing, Visualization, Validation, Supervision, Software, Project administration, Methodology, Investigation, Conceptualization. **Tofael Ahmed:** Writing – review & editing, Supervision, Resources, Methodology, Formal analysis. **Mazaher Karimi:** Writing – review & editing, Visualization, Supervision, Resources, Investigation, Funding acquisition.

Declaration of competing interest

The authors declare that they have no known competing financial interests or personal relationships that could have appeared to influence the work reported in this paper.

Acknowledgment

This research has been supported by University of Vaasa and the DiTArtIS project, "Network of Excellence in Digital Technologies and AI Solutions for Electromechanical and Power Systems Applications" with Grant Agreement number: 101079242 – HORIZON-WIDERA-2021-ACCESS-03.

Data availability

Data will be made available on request.

References

[1] M.H. Rehmani, M. Reisslein, A. Rachedi, M. Erol-Kantarci, M. Radenkovic, Integrating renewable energy resources into the smart grid: recent developments in information and communication technologies, IEEE Trans. Ind. Informat. 14 (2018) 2814–2825, https://doi.org/10.1109/TII.2018.2819169.
[2] Nascimento, R.; Ramos, F.; Pinheiro, A.; Junior, W.d.A.S.; Arcanjo, A.M.C.; Filho, R.F.D.; Mohamed, M.A.; Marinho, M.H.N., "Case Study of Backup Application with Energy Storage in Microgrids," Energies, 15 (2022) 9514, doi:https://doi.org/10.3390/en15249514.
[3] Diambomba Hyacinthe Tungadio, Yanxia sun, "energy stored management of islanded distributed generations interconnected,", J. Energy Storage 44 (2021) 103290 https://doi.org/10.1016/j.est.2021.103290.
[4] M.H. Chehab, C. Ben Salah, R. Falama, R. Zieba, M. Tlija, A. Rabhi, Comparative analysis of energy storage Technologies for Microgrids, Int. Trans. Electr. Energy Syst. 2023 (2023) 6679740, https://doi.org/10.1155/2023/6679740.
[5] Subhashree Choudhury, Review of energy storage system technologies integration to microgrid: types, control strategies, issues, and future prospects, J. Energy Storage 48 (2022) 103966, https://doi.org/10.1016/j.est.2022.103966.
[6] G. Chaudhary, J.J. Lamb, O.S. Burheim, B. Austbø, Review of energy storage and energy management system control strategies in microgrids, Energies 14 (2021) 4929, https://doi.org/10.3390/en14164929.
[7] Kavishka Dissanayake, Dulsha Kularatna-Abeywardana, A review of supercapacitors: materials, technology, challenges, and renewable energy applications, J. Energy Storage 96 (2024) 112563, https://doi.org/10.1016/j.est.2024.112563.
[8] R. Georgious, R. Refaat, J. Garcia, A.A. Daoud, Review on energy storage Systems in Microgrids, Electronics 10 (2021) 2134, https://doi.org/10.3390/electronics10172134.
[9] M. Faisal, M.A. Hannan, P.J. Ker, A. Hussain, M.B. Mansor, F. Blaabjerg, Review of energy storage system Technologies in Microgrid Applications: issues and challenges, IEEE Access 6 (2018) 35143–35164, https://doi.org/10.1109/ACCESS.2018.2841407.
[10] Yujie Wang, Li Wang, Mince Li, Zonghai Chen, A review of key issues for control and management in battery and ultra-capacitor hybrid energy storage systems, eTransportation 4 (2020) 100064, https://doi.org/10.1016/j.etran.2020.100064.
[11] Y. Tahir, M. F. Nadeem, A. Ahmed, I. A. Khan, and F. Qamar, "A Review on Hybrid Energy Storage Systems in Microgrids,", 3rd international conference on computing, mathematics and engineering technologies (iCoMET), Sukkur, Pakistan 2020 (2020) 1–7, https://doi.org/10.1109/iCoMET48670.2020.9073919.
[12] Salman Hajiaghasi, Ahmad Salemnia, Mohsen Hamzeh, Hybrid energy storage system for microgrids applications: a review, J. Energy Storage 21 (2019) 543–570, https://doi.org/10.1016/j.est.2018.12.017.
[13] M.F. Roslan, M.A. Hannan, P.J. Ker, K.M. Muttaqi, T.M.I. Mahlia, Optimization algorithms for energy storage integrated microgrid performance enhancement, J. Energy Storage 43 (2021) 103182, https://doi.org/10.1016/j.est.2021.103182.
[14] A. Bonfiglio, M. Brignone, M. Invernizzi, A. Labella, D. Mestriner, R. Procopio, A simplified microgrid model for the validation of islanded control logics, Energies 10 (2017) 1141, https://doi.org/10.3390/en10081141.
[15] A. Latif, S.M.S. Hussain, A. Al-Durra, A. Iqbal, Hierarchical fuzzy framework for EV supported islanded microgrid frequency stabilization, IEEE Open J. Ind. Electron. Soc. 5 (2024) 704–721, https://doi.org/10.1109/OJIES.2024.3421669.
[16] Smita Sinha, Prabodh Bajpai, Power management of hybrid energy storage system in a standalone DC microgrid, J. Energy Storage 30 (2020) 101523, https://doi.org/10.1016/j.est.2020.101523.
[17] Prashant Singh, Jagdeep Singh lather, "power management and control of a grid-independent DC microgrid with hybrid energy storage system,", Sustain Energy Technol Assess 43 (2021) 100924 https://doi.org/10.1016/j.seta.2020.100924.
[18] Zineb Cabrane, Jonghoon Kim, Kisoo Yoo, Mohammed Ouassaid, HESS-based photovoltaic/batteries/supercapacitors: energy management strategy and DC bus voltage stabilization, Sol. Energy 216 (2021) 551–563, https://doi.org/10.1016/j.solener.2021.01.048.
[19] C.R. Arunkumar, Udaya Bhasker Manthati, Srinivas Punna, "supercapacitor voltage based power sharing and energy management strategy for hybrid energy storage system,", J. Energy Storage 50 (2022) 104232 https://doi.org/10.1016/j.est.2022.104232.
[20] S.A. Al-Salloomee, S. Khosroabadi, A.A. Abdullah Albukariat, Study of power management of standalone DC microgrids with battery supercapacitor hybrid energy storage system, Int. J. Electr. Comput. Eng. 12 (2022) 114–121, https://doi.org/10.11591/ijece.v12i1.pp114-121.
[21] S. Remache, S. El Islam Remache, and K. Barra, "Predictive Power Control and Power Management for Islanded PV Microgrid with Battery-Supercapacitor Hybrid Energy Storage System," 2022 International conference of advanced Technology in Electronic and Electrical Engineering (ICATEEE), M'sila, Algeria, 2022, pp. 1–6, doi:https://doi.org/10.1109/ICATEEE57445.2022.10093742.
[22] S. Punna, S. Banka, S.R. Salkuti, Optimal energy management scheme of battery supercapacitor-based bidirectional converter for DC microgrid applications, Information 13 (2022) 350, https://doi.org/10.3390/info13070350.
[23] Furqan A. Abbas, Adel A. Obed, Mohammed A. Qasim, Salam J. Yaqoob, Seydali Ferahtia, An efficient energy-management strategy for a DC microgrid powered by a photovoltaic/fuel cell/battery/supercapacitor, Clean Energy 6 (2022) 827–839, https://doi.org/10.1093/ce/zkac063.
[24] Suchismita Patel, Arnab Ghosh, Pravat Kumar ray, "efficient power management and control of DC microgrid with supercapacitor-battery storage systems,", J. Energy Storage 73 (2023) 109082 https://doi.org/10.1016/j.est.2023.109082.

[25] Md. Shafiul Alam, Fahad Saleh Al-Ismail, Fahad A. Al-Sulaiman, Mohammad A. Abido, "Energy management in DC microgrid with an efficient voltage compensation mechanism," Electr. Power Syst. Res., 214 (2023) 108842, doi:https://doi.org/10.1016/j.epsr.2022.108842.
[26] Hassan Abouobaida, Lais de Oliveira-Assis, Emanuel P.P. Soares-Ramos, Hassane Mahmoudi, Josep M. Guerrero, Mohsin Jamil, "Energy management and control strategy of DC microgrid based hybrid storage system," Simul. Model. Pract. Theory, 124 (2023) 102726, doi:https://doi.org/10.1016/j.simpat.2023.102726.
[27] S. Sruthi, K. Karthikumar, P. Chandrasekhar, An efficient power management control strategy for grid-independent hybrid renewable energy systems with hybrid energy storage: hybrid approach, J. Energy Storage 95 (2024) 112325, https://doi.org/10.1016/j.est.2024.112325.
[28] H. Zhu, S.A.Z. Ahmed, M.A. Alfakih, M.A. Abdelbaky, A.R. Sayed, M.A.A. Saif, Photovoltaic failure diagnosis using sequential probabilistic neural network model, IEEE Access 8 (2020) 220507–220522, https://doi.org/10.1109/ACCESS.2020.3043129.
[29] S. Ferahtia, A. Djerioui, S. Zeghlache, et al., A hybrid power system based on fuel cell, photovoltaic source and supercapacitor, SN Appl. Sci. 2 (2020) 940, https://doi.org/10.1007/s42452-020-2709-0.
[30] Ali Sayah, Marwa Ben Saïd-Romdhane, Sondes Skander-Mustapha, "Advanced energy management system with road gradient consideration for fuel cell hybrid electric vehicles,", Res. Eng. Des. 23 (2024) 102721 https://doi.org/10.1016/j.rineng.2024.102721.
[31] M. Albakri, A. Darwish, P. Twigg, A comprehensive review of dc/ac single-phase differential-mode inverters for low-power applications, Electronics 13 (2024) 2474, https://doi.org/10.3390/electronics13132474.
[32] S.A.G.K. Abadi, J. Choi, A. Bidram, A method for charging electric vehicles with battery-supercapacitor hybrid energy storage systems to improve voltage quality and battery lifetime in islanded building-level DC microgrids, IEEE Trans. Sustain. Energy 14 (2023) 1895–1908, https://doi.org/10.1109/TSTE.2023.3254597.
[33] O. Diouri, N. Es-Sbai, F. Errahimi, A. Gaga, C. Alaoui, Modeling and design of single-phase PV inverter with MPPT algorithm applied to the boost converter using back-stepping control in standalone mode, Int. J. Photoenergy 2019 (2019) 7021578, https://doi.org/10.1155/2019/7021578.
[34] Maria C. Argyrou, Christos C. Marouchos, Soteris A. Kalogirou, Paul Christodoulides, Modeling a residential grid-connected PV system with battery–supercapacitor storage: control design and stability analysis, Energy Rep. 7 (2021) 4988–5002, https://doi.org/10.1016/j.egyr.2021.08.001.
[35] R. Bakhshi-Jafarabadi, A. Lekić, F.D. Marvasti, J. de Jesus Chavez, M. Popov, Analytical overvoltage and power-sharing control method for photovoltaic-based low-voltage islanded microgrid, IEEE Access 11 (2023) 134286–134297, https://doi.org/10.1109/ACCESS.2023.3336945.
[36] S. Punna, U.B. Manthai, A. Chirayaratil, Modeling, analysis, and design of novel control scheme for two-input bidirectional DC-DC converter for HESS in DC microgrid applications, Int. Trans. Electr. Energy Syst. e12774 (2023), https://doi.org/10.1002/2050-7038.12774.